



Contents lists available at ScienceDirect

# Journal of Geodynamics

journal homepage: <http://www.elsevier.com/locate/jog>



## Implications for anomalous mantle pressure and dynamic topography from lithospheric stress patterns in the North Atlantic Realm

Christian Schiffer<sup>a,b,\*</sup>, Søren Bom Nielsen<sup>a</sup>

<sup>a</sup> Department of Earth Sciences, Durham University, Durham, United Kingdom

<sup>b</sup> Department of Geoscience, Aarhus University, Aarhus, Denmark

### ARTICLE INFO

#### Article history:

Received 31 January 2016

Received in revised form 21 March 2016

Accepted 27 March 2016

Available online xxx

#### Keywords:

Geodynamics

Lithospheric stress field

Thermo-isostatic modelling

Gravitational potential energy

North Atlantic

### ABSTRACT

With convergent plate boundaries at some distance, the sources of the lithospheric stress field of the North Atlantic Realm are mainly mantle tractions at the base of the lithosphere, lithospheric density structure and topography. Given this, we estimate horizontal deviatoric stresses using a well-established thin sheet model in a global finite element representation. We adjust the lithospheric thickness and the sub-lithospheric pressure iteratively, comparing modelled in plane stress with the observations of the World Stress Map. We find that an anomalous mantle pressure associated with the Iceland and Azores melt anomalies, as well as topography are able to explain the general pattern of the principle horizontal stress directions. The Iceland melt anomaly overprints the classic ridge push perpendicular to the Mid Atlantic ridge and affects the conjugate passive margins in East Greenland more than in western Scandinavia. The dynamic support of topography shows a distinct maximum of c. 1000 m in Iceland and amounts <150 m along the coast of south-western Norway and 250–350 m along the coast of East Greenland. Considering that large areas of the North Atlantic Realm have been estimated to be sub-aerial during the time of break-up, two components of dynamic topography seem to have affected the area: a short-lived, which affected a wider area along the rift system and quickly dissipated after break-up, and a more durable in the close vicinity of Iceland. This is consistent with the appearance of a buoyancy anomaly at the base of the North Atlantic lithosphere at or slightly before continental breakup, relatively fast dissipation of the fringes of this, and continued melt generation below Iceland.

© 2016 Elsevier Ltd. All rights reserved.

## 1. Introduction

The geological evolution and the geodynamic state of North Atlantic Realm (NAR) has inspired some of the most fundamental ideas and discussions in Earth Science such as plate and plume hypotheses, continental break up mechanisms, supercontinent cycles, dynamic topography, and erosion and isostasy.

Particularly conspicuous are the topographic and magmatic anomalies associated with the Iceland melt anomaly. The main point of discussion is whether or not a mantle plume is the cause of these features or if the causative agent is of a more shallow nature (Morgan, 1971; Anderson, 2001; Meyer et al., 2007).

Different methods are used to test the proposed hypotheses in the NAR. Seismic tomography methods map seismic wave speed anomalies in the crust, upper and lower mantle on different scales

(Foulger et al., 2001; Darbyshire et al., 2004; Weidle and Maupin, 2008; Köhler et al., 2011; Medhus et al., 2012; Zhu et al., 2012; Rickers et al., 2013; Schaeffer and Lebedev, 2013; Hejrani et al., 2015). However, P- and S-wave velocities strongly depend on a number of factors such as temperature, composition and the presence of volatiles (Cammarano et al., 2003; Hier-Majumder, 2008; Xu et al., 2008) and often lack repeatability (Foulger et al., 2015), and model resolution is limited by data coverage and processing parameters (Foulger et al., 2013; Rawlinson et al., 2014). Receiver functions (Darbyshire et al., 2000; Dahl-Jensen et al., 2003; Foulger et al., 2003; Kumar et al., 2005, 2007; Svennengsen et al., 2007; Kolstrup and Maupin, 2013; Schiffer et al., 2014, 2015a) and active source seismic experiments, often in combination with gravity and magmatic modelling (Fichler et al., 2011; Nirrengarten et al., 2014; Gernigon et al., 2015) image the crustal and lithospheric structure and allow an interpretation of its evolution. Geochemistry and petrology give insight into the orogenic and magmatic evolution and origin of rocks and melts (Saunders et al., 1997; Tegner et al., 1998; Korenaga and Kelemen, 2000; Brown and Lesher, 2014). In

\* Corresponding author at: Department of Earth Sciences, Durham University, South Road, Durham DH1 3LE, United Kingdom

E-mail address: [christian.schiffer@zoho.com](mailto:christian.schiffer@zoho.com) (C. Schiffer).

spite of these efforts, the debate on the origin of the North Atlantic Igneous Province (NAIP) and distinct landforms is still ongoing.

Dynamic topography is the direct effect of sub-lithospheric pressure anomalies related to mantle convection patterns acting at the base of the lithosphere (e.g. Höink and Lenardic, 2010; Höink et al., 2011). However, deriving estimates of dynamic topography from the available data is not trivial. Velocity anomalies in the upper mantle mapped by seismic tomography have been associated with dynamic topography patterns (Conrad et al., 2004; Moucha and Forte, 2011; Flament et al., 2013; Ricker et al., 2013), but because of the mentioned ambiguity of seismic velocities, tomography in itself is usually insufficient to corroborate proposed cases for vertical movements. Dynamic topography is also often derived from the residual topography, the difference between the isostatic response of a crustal or lithospheric density model and observed topography. Molnar et al. (2015) emphasised that residual topography and dynamic topography are not equivalent since the residual topography includes also other isostatic effects.

In this study, we constrain dynamic topography by modelling gravitational lithospheric stresses in the presence of sub-lithospheric mantle pressure. Initial model realisations are based on the observed residual topography, but modified in terms of amplitude and wavelength. These are tested and iteratively optimised by comparing their stress predictions to the World Stress Map (WSM). The results give an independent estimate of absolute magnitude and lateral extent of the mantle pressure anomaly and the accompanying dynamic topography with focus on the NAR. The NAR is ideal for the approach because convergent plate boundaries are far away and affect the region only by a relatively uniform far-field stress. This leaves the dominant stress sources to topography, lithospheric density structure, and mantle tractions. Furthermore, as relatively good global models of lithospheric thickness variations and crustal structure are available, the lithospheric stress field can be considered a robust observable and measure of lithospheric and upper mantle structure in the NAR.

## 2. Geological setting

The tectonic evolution of the NAR includes at least two complete Wilson cycles. The most recent was initiated by the closure of the Iapetus Ocean culminating in the Ordovician to Early Devonian Caledonian orogeny (Roberts, 2003; Gee et al., 2008; Leslie et al., 2008). The subsequent approximately 340 Myr lasting period of post-orogenic collapse and extension of the Caledonian mountain range (Andersen et al., 1991; Dewey et al., 1993; Fossen, 2010) transitioned into active rifting and finally continental break-up and sea-floor spreading in the early Cenozoic (Skogseid et al., 2000; Nielsen et al., 2007; Gernigon et al., 2015). North Atlantic break-up was accompanied by a large magmatic outburst and the formation of the North Atlantic Igneous Province (Saunders et al., 1997). This magmatic event is commonly associated to a mantle plume (e.g. Fitton et al., 1997; Tegner et al., 1998) but also shallower, plate tectonic origins are proposed (e.g. Korenaga, 2004; Foulger et al., 2005; Schiffer et al., 2015b).

This complex history shaped the NAR and its different tectonic domains (oceanic, transitional, orogenic, cratonic) (Fig. 1), which show significant variation in age, crustal and lithospheric structure, composition and thermal state (Darbyshire et al., 2004; Artemieva et al., 2006; Gee and Stephenson, 2006; Grad et al., 2009; Artemieva and Thybo, 2013). The magma-rich passive continental margins form the transition from oceanic crust and lithosphere to the North American and European continents, which have old Precambrian Cratons with thick crust and lithosphere as the stable core (Gee and Stephenson, 2006; Artemieva et al., 2006). Phanerozoic Central and Western Europe comprises uniformly thin crust

and lithosphere (Ziegler and Dèzes, 2006). Thickened crust underlies the active Alpine Orogen (Gee and Stephenson, 2006; Stamfli and Kozur, 2006). The North Atlantic Ocean shows significant complexity including anomalously high elevation and thick crust in the vicinity of Iceland (Larsen and Saunders, 1998; Foulger et al., 2000), rifted continental slivers, asymmetric continental shelves and an inactive spreading ridge (Lundin and Doré, 2011; Gernigon et al., 2015).

The North Atlantic passive margins are accompanied by distinct high-elevation, low-relief topography in East Greenland and Scandinavia, the origin of which is matter of debate (Anell et al., 2009; Nielsen et al., 2009; Pascal and Olesen, 2009; Chalmers et al., 2010). The occurrence of these landscapes has been explained by peneplains uplifted to their present elevation in the Neogene (Japsen and Chalmers, 2000; Lidmar-Bergström and Näslund, 2002; Green et al., 2013). Others have suggested that the landscapes are remains of the Caledonian mountain range, modified by climatically controlled erosion and not the least glacial and periglacial processes (Egholm et al., 2009; Nielsen et al., 2009; Pedersen et al., 2010).

In western Scandinavia, the isostatic compensation of the crust and lithosphere, as well as its age and composition, lend strong support to the hypothesis of long lived topography (Balling, 1980; Ebbing et al., 2012; Gradmann et al., 2013; Maupin et al., 2013). Neogene uplift also has been proposed for East Greenland (Japsen et al., 2010, 2013, 2014; Bonow et al., 2014) and, undoubtedly, south and central East Greenland was heavily affected by early Cenozoic break-up magmatism, especially in the Scoresbysund area, but this was well before the Neogene. For other areas of the East Greenland Caledonides, the available data suggest thick crust (Braun et al., 2007; Artemieva and Thybo, 2013; Schiffer et al., 2014, 2015a and references therein), which has provided support of the topography since its creation by orogenesis. In Northeast Greenland, apatite fission track modelling suggest no extreme vertical motions for most of the Mesozoic and Cenozoic, other than post-glacial flexural isostatic uplift (Pedersen et al., 2012). Obviously, all margins have been additionally affected by the glacial carving of fjords and associated flexural isostatic uplift (Gilchrist and Summerfield, 1990; Medvedev et al., 2008, 2013; Medvedev and Hartz, 2015).

## 3. The lithospheric stress field in the North Atlantic Realm

The lithospheric stress field is the consequence of a number of stress sources including ridge push and slab pull, radial and horizontal drag of the convecting mantle at the base of the lithosphere, thermal stresses, pressure differences due to lateral variation in the density structure of the lithosphere, as well as a number of resistive forces (Ranalli, 1995; Bird et al., 2008; Naliboff et al., 2012). The stresses most prominently manifest at convergent and translational plate boundaries released by earthquakes. Dynamic topography caused by vertical sub-lithospheric tractions has a major effect on the geopotential stress field because of the larger pressure of the elevated lithospheric column (Steinberger et al., 2001; Lithgow-Bertelloni and Guynn, 2004). Therefore, the stress field contains information on the extent and amplitude of dynamic uplift, especially in regions where stress release at convergent plate boundaries are absent, such as in the NAR.

The stress field in the NAR shows large variation between different regions (Müller et al., 1992). The closest convergent plate boundary is the Alpine fold belt, the result of generally north-south convergence of Africa and Europe (Rosenbaum et al., 2002). The compression acts as a counterpart to the North Atlantic ridge push (Grünthal and Stromeyer, 1992; Gölke and Coblenz, 1996), and this system causes the relatively uniform NW-SE to NNW-SSE directed far-field stress and also intraplate deformation in Central Europe (Marotta et al., 2002; Kaiser et al., 2005; Jarosiński et al., 2006).

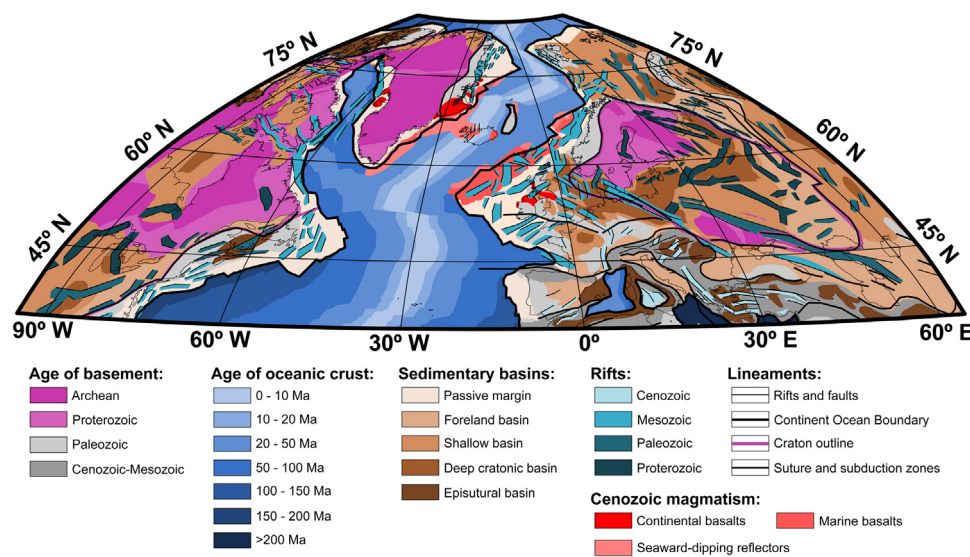


**Fig. 1.** Tectonic Map of the North Atlantic Realm (modified from Roberts and Bally, 2012 and Larsen and Saunders, 1998) showing the age of the basement and oceanic lithosphere, basins, rifts, magmatic products and major tectonic lineaments. An equal-area Hammer-Aitoff projection is chosen for the visualisation of this as well as all following maps, drawn with the MATLAB package M.Map (<http://www.eos.ubc.ca/~rich/map.html>).

The stress field of Northern Europe is further influenced by the East European Craton, the high topography of the Scandinavian Caledonides and ridge push from the North Atlantic. Post-glacial uplift causes significant low-magnitude seismicity and a disturbance of the regional stress field (Marquart, 1989; Müller et al., 1992; Wu et al., 1999; Bungum et al., 2010). Pascal and Cloetingh (2009) have illustrated that the geopotential effect of the lithospheric structure, especially of the Scandinavian Caledonides, has a major effect on the stress field of the Norwegian continental margin, concurrent with the ridge push. The thick oceanic crust and high topography beneath the Greenland-Scotland ridge and Iceland causes perturbations of the ridge push force along the North Atlantic Ridge (Bott, 1991; Nielsen et al., 2014).

#### 4. Global modelling approach

This section describes the governing equations and the analytical methods that allow constraining the lithospheric structure and the mantle pressure anomaly by the World Stress Map. The modelling is global, but we only discuss results in the NAR. Models and figures are, therefore, only shown for the NAR, although similar changes are made globally, but are not matter of discussion in the paper.

##### 4.1. Thin sheet approximation and stress prediction

The horizontal gradient of the geopotential energy (GPE) is a source of deviatoric stress. The GPE itself is the first moment of the vertically integrated density anomaly,  $\Delta\rho$ , with respect to a reference lithosphere:

$$GPE = \int_{-E}^L (L-z)\Delta\rho \times g dz \quad (1)$$

In Eq. (1) L is a reference depth, E the topographic elevation and g is the gravitational acceleration.

Vertical displacement of the lithosphere by a mantle pressure anomaly changes the GPE. Assuming that horizontal gradients of lithospheric structure are small leads to the thin sheet approximation of the lithosphere (Bird and Piper, 1980; England and McKenzie, 1982; England and Houseman, 1986), which shows how horizontal GPE gradients are a source of deviatoric horizontal litho-

spheric stress. The general approach is similar to that presented in Neves et al. (2014) and the governing equations read:

$$\begin{pmatrix} \frac{\partial \bar{\tau}_{xx}}{\partial x} + \frac{\partial \bar{\tau}_{xy}}{\partial y} + \frac{\partial \bar{\tau}_{xz}}{\partial z} - \frac{\partial \bar{\tau}_{zz}}{\partial x} = -\frac{1}{L} \left( \frac{\partial GPE}{\partial x} \right) \\ \frac{\partial \bar{\tau}_{yx}}{\partial x} + \frac{\partial \bar{\tau}_{yy}}{\partial y} + \frac{\partial \bar{\tau}_{yz}}{\partial z} - \frac{\partial \bar{\tau}_{zz}}{\partial y} = -\frac{1}{L} \left( \frac{\partial GPE}{\partial y} \right) \end{pmatrix} \quad (2)$$

here, x and y are local horizontal coordinates,  $\bar{\tau}$  represents depth integrated deviatoric stresses,  $\bar{\tau}_{xx}$ ,  $\bar{\tau}_{yy}$ ,  $\bar{\tau}_{xy}$  are horizontal deviatoric stresses, and  $\bar{\tau}_{zz}$  is a sub-lithospheric pressure anomaly acting vertically at the base of the lithosphere (radial tractions).

Since horizontal tractions at the surface by assumption are zero, integration of  $\bar{\tau}_{xz}$  results in  $\tau_{xz}(L)$  and  $\bar{\tau}_{yz}$  in  $\tau_{yz}(L)$

$$\begin{pmatrix} \frac{\partial \bar{\tau}_{xx}}{\partial x} + \frac{\partial \bar{\tau}_{xy}}{\partial y} = \frac{1}{L} \left( \frac{\partial GPE}{\partial x} + L \frac{\partial \bar{\tau}_{zz}}{\partial x} \right) - \tau_{xz}(L) \\ \frac{\partial \bar{\tau}_{yx}}{\partial x} + \frac{\partial \bar{\tau}_{yy}}{\partial y} = \frac{1}{L} \left( \frac{\partial GPE}{\partial y} + L \frac{\partial \bar{\tau}_{zz}}{\partial y} \right) - \tau_{yz}(L) \end{pmatrix} \quad (3)$$

Horizontal tractions at the base of the lithosphere therefore contribute to the source term on the right hand side of Eq. (3). They are the result of dynamic processes and convection patterns in the sub-lithospheric mantle and require the existence of a mechanical coupling between lithosphere and the convective currents. Numerical simulations have shown that different flow modes are active depending on lithospheric strength and lithosphere-asthenosphere coupling. A flow driven by pressure gradient in the asthenosphere with a stagnant lid acting at short wavelengths (Poiseuille flow), contrasting a flow mode with an active, moving lid at longer wavelength (Couette flow) (Höink and Lenardic, 2010). In the NAR, pressure driven Poiseuille flow is more likely to be in place, in the absence of a slab-pull component (Höink et al., 2011). Estimates of horizontal mantle tractions must be based on assumptions about mantle convection patterns, viscosity models and lithosphere-asthenosphere coupling (Ghosh et al., 2008; Naliboff et al., 2009; Ghosh and Holt, 2012). Either of these quantities is connected with considerable error bars and to minimise the number of unknowns and potential error sources, we decide to neglect horizontal mantle tractions at the base of the lithosphere

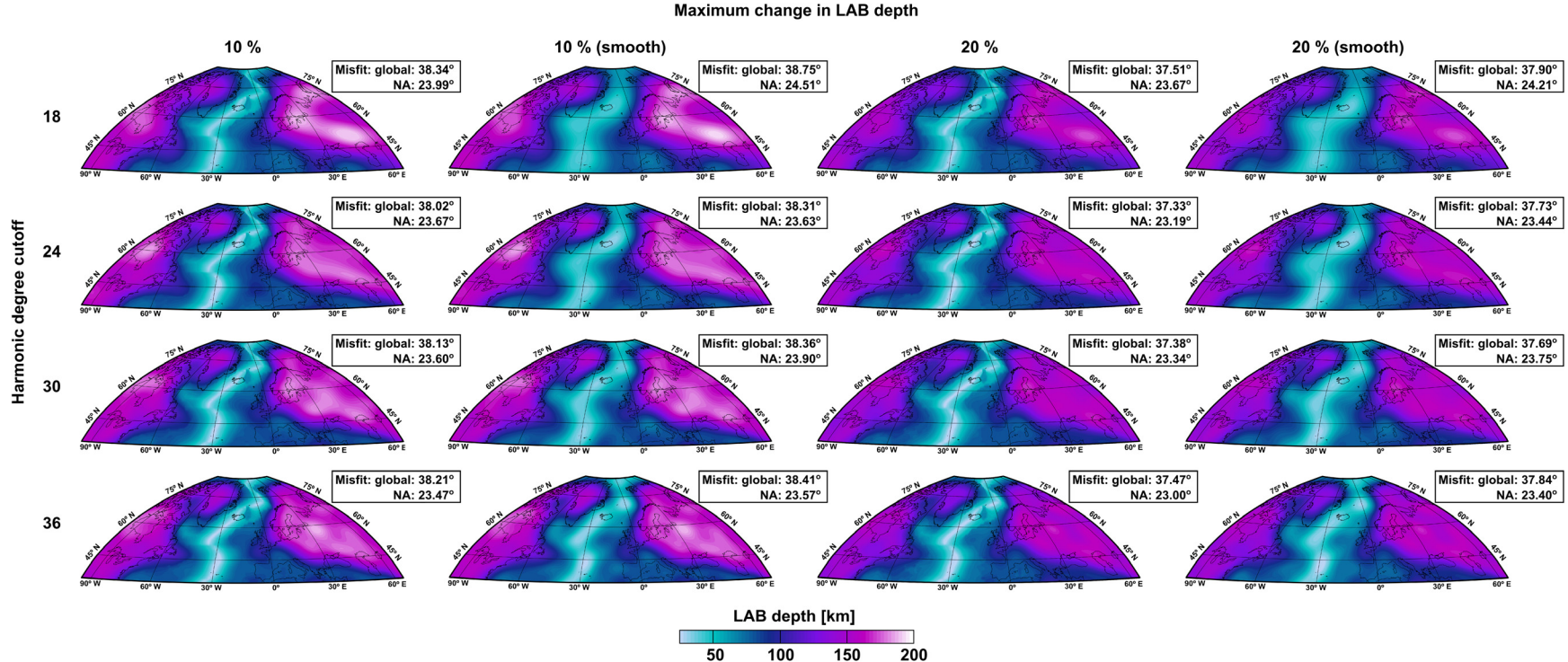


**Fig. 2.** Sixteen LAB depth starting models. All models are created based on the observed residual topography. Different model variations are created by limiting the maximum change of 10% (left) or 20% (right) of the reference LAB depth (x-direction). One set of 8 models are the original harmonic expansion models (described in the text) and another 8 models maintain partly the theoretical ocean-age based depth for the oceanic lithosphere, thereby maintaining a steep continent-ocean transition. The models show also LAB depth changes of different wavelength, indicated by the maximum degree of the harmonic expansion (y-direction).

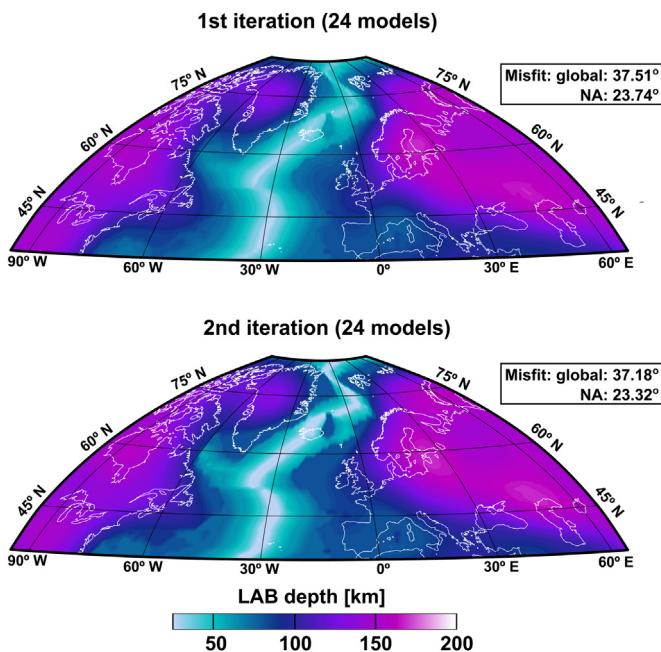


**Fig. 3.** Best fitting LAB depth models after the first and second iteration. The third iteration did not result in a better fit.

( $\tau_{xz}(L) = 0$ ,  $\tau_{yz}(L) = 0$ ), so that the simplified equations used in the present analysis read:

$$\begin{cases} \frac{\partial \bar{\tau}_{xx}}{\partial x} + \frac{\partial \bar{\tau}_{xy}}{\partial y} = -\frac{1}{L} \left( \frac{\partial GPE}{\partial x} + L \frac{\partial \bar{\tau}_{zz}}{\partial x} \right) \\ \frac{\partial \bar{\tau}_{yx}}{\partial x} + \frac{\partial \bar{\tau}_{yy}}{\partial y} = -\frac{1}{L} \left( \frac{\partial GPE}{\partial y} + L \frac{\partial \bar{\tau}_{zz}}{\partial y} \right) \end{cases} \quad (4)$$

Although the radial mantle tractions  $\bar{\tau}_{zz}$  explicitly appear in Eq. (4), we follow here the discussion of Ghosh et al. (2008) and include it into the lithospheric density model as a source for dynamic topography of the lithospheric column. The calculated dynamic geopotential energy,  $GPE_{dyn}$ , is the geopotential energy of an uplifted lithospheric columns and equivalent to the GPE of an isostatically compensated lithosphere, plus a term representing the pressure anomaly,  $\bar{\tau}_{zz}$ , that such that  $GPE_{dyn} = GPE + \bar{\tau}_{zz} \times L$ .

The  $GPE_{dyn}$  is determined by integrating from the surface position  $-E$  to a depth of  $L=100$  km (Eq. (4)), which is a common approach in a number of studies (Flesch et al., 2001; Ghosh et al., 2008, 2009). Bird et al. (2008) included plate boundary stresses and a number of other global and regional studies using slightly different approaches and assumptions have been published, many of them during the last decade (Flesch and Kreemer, 2010; Ghosh and Holt, 2012; Ghosh et al., 2013).

The equations of equilibrium of stresses (Eq. (4)) with the assumptions and approximations of this study are solved using the Finite Element Method (FEM) in the following way (Zienkiewicz, 1977, Chap. 16): The spherical Earth is represented by a dense grid of flat, thick, triangles with an elastic rheology. Each triangle has 15 degrees of freedom arising from the three corner nodes, each with three spatial coordinates (9 degrees of freedom), and the vertical axis through each node, which has two angular degrees of freedom (6 degrees of freedom). This axis points initially toward the centre of the sphere. After loading the axis can deviate slightly from the vertical as measured by the (small) angles. Zienkiewicz (1977, chap. 16), specifies the relationship between strains and stresses for this thick element. The material parameters of each element comprise Young's modulus, Poisson's ratio and a uniform thickness,  $L$ . The thickness of the elastic shell may be discussed; however, current

models of global laterally varying elastic thickness variation are poorly constrained. In order to avoid additional and unpredictable error sources, a globally constant elastic thickness is assumed. Further, the absolute thickness of a uniform shell does not cause any changes in the orientation of the stress field, only in amplitude. Since the stress field is only compared to the WSM by the orientation, the thickness has no effect in the model. The finite element approach is three-dimensional, and the stress equations are solved in this global Cartesian three-dimensional coordinate system. After solution the stresses are transformed to the local coordinate system with locally horizontal coordinate axis and a vertical axis pointing toward the centre of the sphere. The principle stress directions can now be compared with the World Stress Map.

#### 4.2. Description of modelling procedure

Calculation of GPE of Eq. (4) (or  $GPE_{dyn}$ ) calls for a model of lithospheric structure. Here we used model CRUST1.0 (Laske et al., 2013) as an initial reference for the crustal structure, a seismologically based LAB depth model for continental areas, and a standard ocean age dependent plate model for oceanic lithosphere (Stein and Stein, 1992; Gung et al., 2003; Conrad and Lithgow-Bertelloni, 2006). Using this reference lithospheric structure isostatically balanced with a standard mid-ocean ridge (an adiabatic mantle beneath 2500 m of air, e.g. Lachenbruch and Morgan, 1990) resulted in a topography misfit, termed the residual topography. Being aware of the different definitions of residual and dynamic topography (Molnar et al., 2015), this residual topography can have basically three causes: First, a mantle pressure anomaly could be required; second, the reference lithospheric model could be incorrect; third, the assumption of local isostasy has failed because, for example, flexural effects are important.

Initially discarding the second and third possibilities we used this residual topography to define mantle pressure and LAB depth changes that improved the agreement between observed and predicted topography. We represented the mantle pressure anomaly and the changes to the LAB by spherical harmonics and limited them to be relatively long wavelength and of chosen maximum amplitude (see Section 4.3). The remaining topographic residual was accommodated by small, local changes of other parameters that determine the lithospheric model (layer thickness, densities, and thermal parameters in the crust). We performed these local adjustments of the given parameters using least squares inversion (Tarantola and Valette, 1982) and forward thermal-isostatic lithospheric modelling (see Section 4.3 below). Surface heat flow was according to Pollack and Chapman (1977) and Chapman (pers. comm.).

Once a lithospheric model fulfilled topographic elevation, it was used for the calculation of the horizontal gradients of the thus obtained lithospheric potential energy. The produced global stress prediction was compared with the World Stress Map. By iteratively testing different model combinations of pressure and LAB depth, the global stress prediction was improved and the most suitable model combination determined.

In summary, the modelling procedure involved the following steps:

- (1) Define residual topography by balancing the reference crustal (CRUST 1.0) and LAB models isostatically against a standard mid ocean ridge
- (2) Use this residual topography to determine 16 LAB depth models and 16 pressure models,  $P$ , each with a different combination of maximum amplitude and wavelength (Section 4.3).
- (3) These different models do not exactly reproduce topography because they are relatively long wavelength. To achieve the final topography prediction we adjust for each of the LAB and  $P$

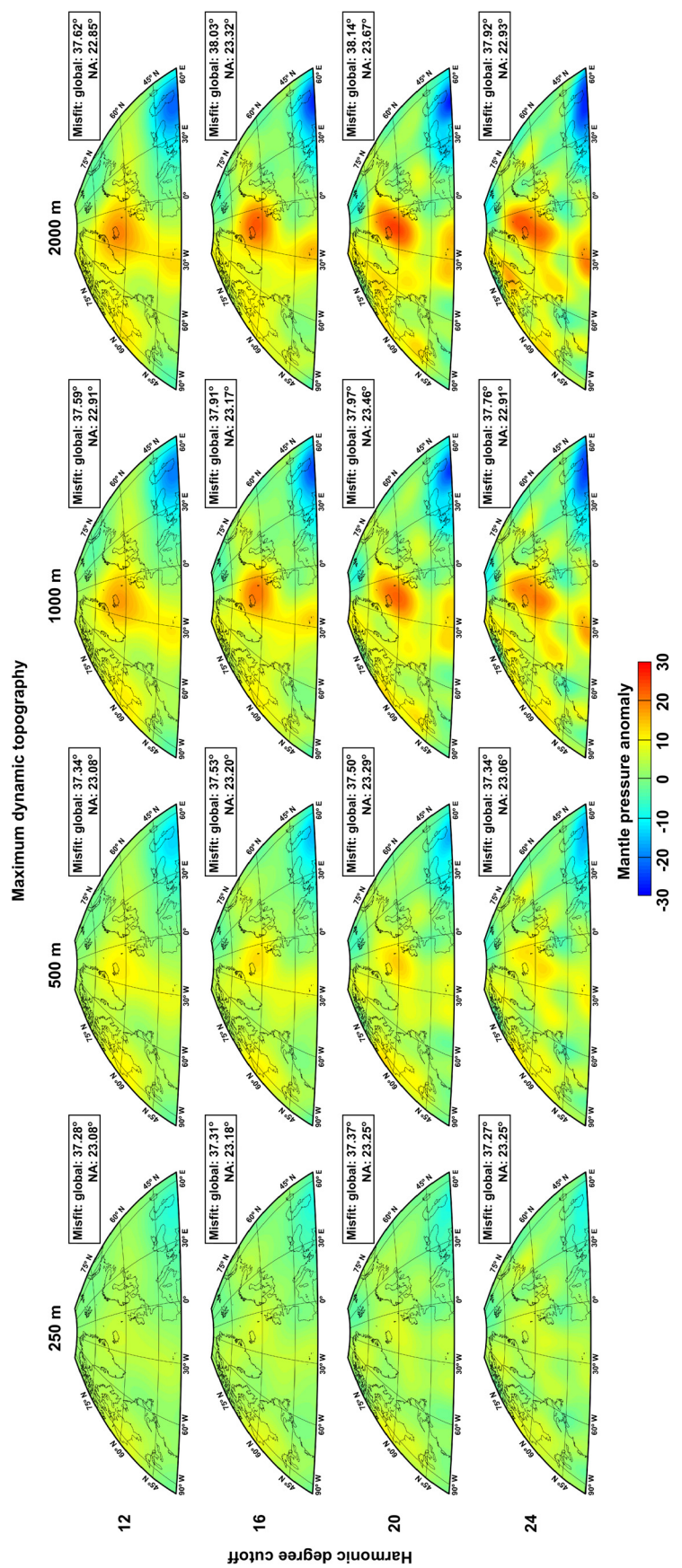


**Fig. 4.** Sixteen sub-lithospheric pressure starting models. All models are created based on the observed residual topography. Different variations are created by limiting the amplitude of the caused dynamic topography (x-direction) and the wavelength or maximum degree of the harmonic expansion (y-direction).

combinations the remaining free parameters, which are mainly densities and layer thicknesses of CRUST 1.0. The final topography prediction is accurate within a few meters for each of the LAB and P models (see Section 4.4 below on how to construct the 16 starting models).

- (4) For each of the models calculate GPE<sub>dyn</sub>
- (5) For each GPE<sub>dyn</sub> calculate stress directions
- (6) Compare the calculated stress directions with the WSM. Some models are better than others, and the final step is an iteration in which:
- (7) New P and LAB models are produced by combinations of the best of the 16 pressure and 16 LAB models. The best fitting models in different defined areas (45° longitudinal and latitudinal areas) are combined and smoothed.

The stress field is recalculated and updated and step (4)–(7) are repeated. This way of “testing”, “combining” and “optimising” is performed by three iterations for LAB and five for pressure until no improvements in the stress field predictions can be noticed.

Further details of the modelling procedure follow below.

#### 4.3. Thermo-isostatic lithospheric model

A layered, one-dimensional thermal model isostatically balanced with a standard mid-ocean ridge was used to predict topography and surface heat flow for each lithospheric column. The steady state geotherm for each layer of constant parameters from the surface to LAB depth was calculated according to

$$T(z) = -\frac{A}{2\lambda}z^2 + \frac{q_0}{\lambda}z + T_0 \quad (5)$$

The symbols are heat production rate A [W kg<sup>-1</sup>], thermal conductivity  $\lambda$  [W m<sup>-1</sup> K<sup>-1</sup>], heat flow at the upper interface  $q_0$  [W m<sup>-2</sup>], as well as the temperature at the upper interface  $T_0$  [°C] of each layer. The temperature at LAB depth,  $T_{LAB}$ , and at the surface,  $T_S$ , allow for solving the system of linear equations. The influence of LAB depth on  $T_{LAB}$  is accommodated by using a standard mantle adiabate of  $[\partial T/\partial z]_a = 0.6^\circ\text{C}/\text{km}$  (McKenzie and Bickle, 1988), and a reference potential temperature,  $T_p = 1315^\circ\text{C}$  (McKenzie et al., 2005). The surface temperature  $T_S$  is 0 °C. Literature values of thermal conductivity and heat production were assigned for oceanic and continental crustal layers, sediments and mantle lithosphere (Turcotte and Schubert, 2002). The conductivity was assumed to be temperature dependent and adjusted accordingly (after Petrunin and Popov, 1995; McKenzie et al., 2005).

The density of the sub-crustal lithosphere between Moho and LAB was defined by thermal expansion of peridotite in the presence of the estimated 1D steady state geotherm (McKenzie et al., 2005). The equation of state for density

$$\rho(\Delta T) = \rho_{ref}(1 - \alpha \Delta T) \quad (6)$$

describes the change of a reference density  $\rho_{ref} = 3350 \text{ km/m}^3$  with regard to a temperature change  $\Delta T$  [°C], which is dependent on the thermal expansion coefficient  $\alpha$  [K<sup>-1</sup>] (Turcotte and Schubert, 2002).  $\alpha$  was also considered temperature dependent (Bouhifd et al., 1996). A priori values of sedimentary and crustal densities were based on CRUST1.0, and here no thermal expansion was assumed.

Isostatic compensation (including a dynamic component) with regard to a reference density structure (Lachenbruch and Morgan, 1990), defined by an adiabatic asthenosphere below a layer of 2500 m of air (“free asthenosphere surface”), gave an estimate of the topography in the presence of a sub-lithospheric pressure anomaly  $\tau_{zz}$  (Eq. (4)). The near-surface temperature gradient and thermal conductivity were used to calculate surface heat flow according to  $q_s = \Delta T / \Delta z \times \lambda$ .

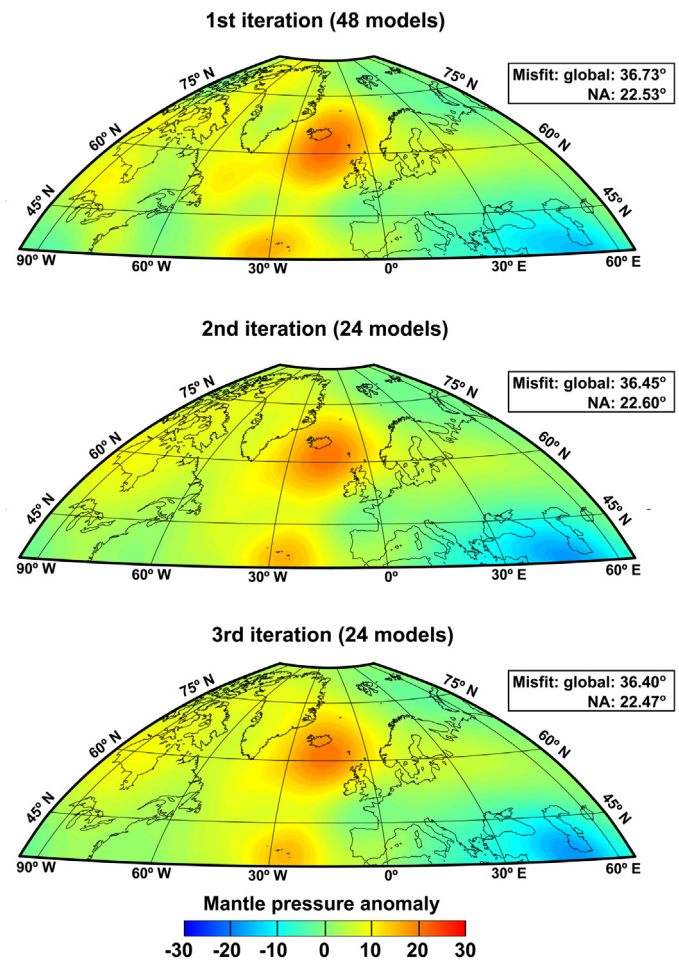


**Fig. 5.** Best fitting sub-lithospheric pressure models after the first to third iteration. The fourth and fifth iteration did not result in a better fit.

Geochemical studies suggest that a higher mantle pressure is associated with slightly elevated mantle temperatures (e.g. Brown and Lesher, 2014). We therefore invoked a weak linear coupling between pressure anomaly and potential temperature of 50 °C per 25 MPa and a negative relation, accordingly, such that  $T_p = 1315^\circ\text{C} + 50^\circ\text{C} \times \Delta P/25 \text{ MPa}$ . This roughly corresponds to a thermal buoyancy anomaly, distributed in the upper mantle.

#### 4.4. LAB depth and sub-lithospheric pressure adjustments

To explain the long wavelength components of the global residual topography we defined initial mantle pressure anomalies and LAB depth changes, which were characterised by different wavelengths and amplitudes.

Lithospheric thickness is less well known and exhibits some dependency on the method which has been used for the mapping (receiver functions, seismic tomography, surface waves, mantle Xenoliths, thermal and electromagnetic modelling, and elasticity) (Fischer et al., 2010; Artemieva, 2009). These methods generally resolve longer wavelength structures.

We wished to allow for this uncertainty in the LAB depth to explain some of the initial residual topography. This was done by changing the LAB depth globally by applying observed change of topography with LAB depth,  $\Delta \text{topo}/\Delta \text{LAB}$  for every point of the model. Because all of the residual topography could in principle be consumed by changes in the LAB depth, and because this end member model is not realistic, we limited LAB depth changes to a maximum change of either 10% or 20%. To obtain a long wave-

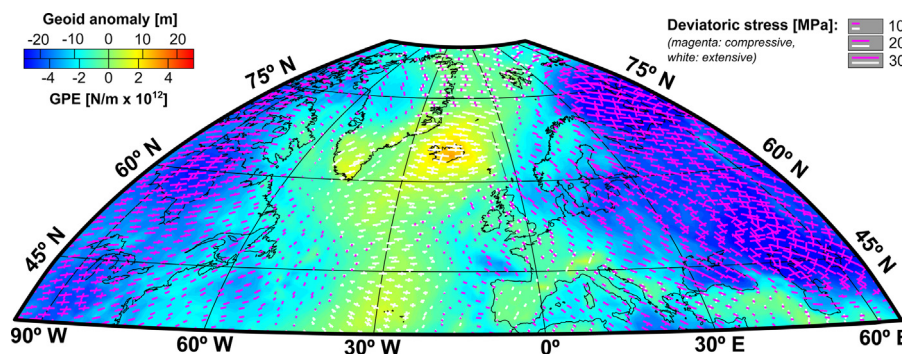


**Fig. 6.** Synthetic Geoid and corresponding GPE of the upper 100 km of the lithospheric model with superimposed principle horizontal stress directions.

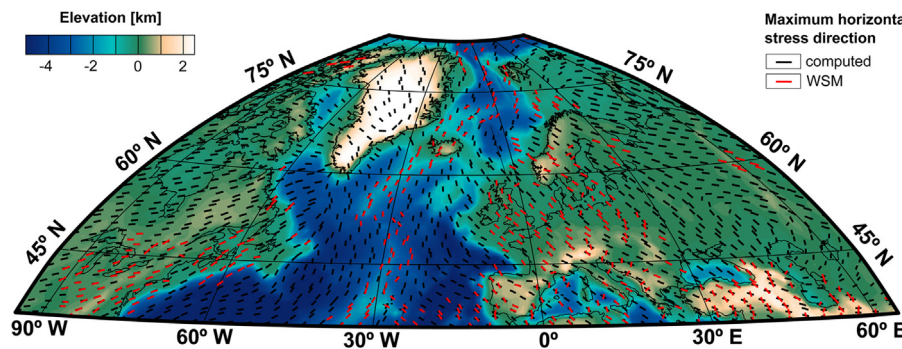


**Fig. 7.** Topography and Maximum horizontal stress directions (at each 4th grid point) of the computed stress field (black) and the World Stress Map (red). Each red bar has a black bar associated with it. In many cases the red bar entirely shadows the underlying black bar. (For interpretation of the references to color in this figure legend, the reader is referred to the web version of this article.)

length adjustment these changes were transformed by Legendre functions into least squares spherical harmonic models, with a cut-off at different maximum degrees (18, 24, 30 and 36) (Fig. 2, “smooth”). Thereby, the longest wavelengths (degrees < 18) were present in all models, whereas the short wavelength content varies. This approach resulted in eight new LAB depth models. Eight further models were created by taking the average of the estimated oceanic lithosphere with a standard plate model (Stein and Stein, 1992) using ocean age models (Müller et al., 2008), in order to maintain a steep gradient at continent-ocean boundaries (COB) (Fig. 2, not “smooth”).

These 16 initially defined models acted as individual starting models for the lithospheric density modelling. The resulting GPE models were then used to calculate the synthetic geopotential stress field. Depending on the misfit to the World Stress Map (WSM), better fitting models were accepted in different regions of the globe. Areas of  $45^\circ \times 45^\circ$  were defined in which each model was evaluated. The best fitting models were kept in each region and again smoothed using the four previously used ranges of harmonic degrees (cut-off at 18, 24, 30 or 36). Another set of models was produced by using defined areas, shifted by  $22.5^\circ$  as compared to the previous ones. This successively improved the global fit of the stress field. After the second iteration, however, no further improvement was noticed, so that after three iterations and a total of 72 tested models, the procedure was terminated (see Fig. 3).

Mantle pressure anomalies were defined in a similar way to consume the remaining long-wavelength residual topography (using  $\Delta P/\Delta \text{topo}$ ). Here slightly larger wavelengths, expressed by the sum of harmonic degrees of the fundamental model up to a maximum harmonic degree of 12, 16, 20 and 24 were created and the amplitude was limited to a maximum dynamic topography of 250, 500, 1000 and 2000 m, resulting in 16 individual models (Fig. 4). The models were analysed in terms of the agreement with the WSM and

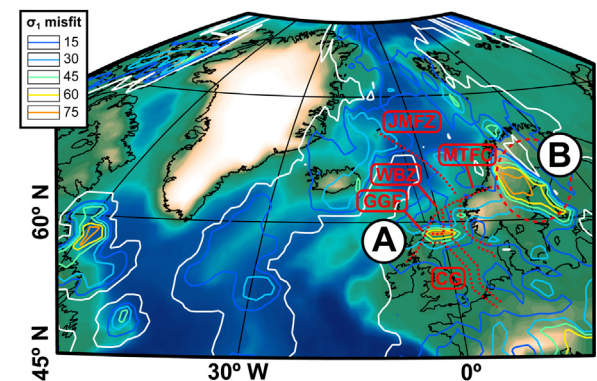


**Fig. 8.** Topography and stress field misfit contour lines (degrees); dotted red lines: major faults (JMFZ: Jan Mayen Fracture Zone; GGF: Great Glen Fault; WBZ: Walls Boundary Fault; MTFC: Møre Trøndelag Fault Complex; CG: Central Graben from Fossen (2010)). Digital Tectonic Activity Map of the Earth; stippled red line: 5 mm/a postglacial rebound isoline (Balling, 1980). (For interpretation of the references to color in this figure legend, the reader is referred to the web version of this article.)

recombined and averaged in the same areas as for the LAB models ( $45^\circ \times 45^\circ$  areas and a set of areas shifted by  $22.5^\circ$ ). Five iterations were performed (with a total of 120 tested models); however, already after the 3rd iteration no further improvement of the stress field was achieved, indicating a convergence to a unique solution (Fig. 5), and the best fitting global model was defined.

This simple iterative optimisation approach to explore new LAB and pressure models was very effective and increased the agreement between the computed stress field and the WSM. It must be emphasised that all models were based on the initially calculated residual topography. Since the initial residual topography model was based on the chosen isostatic forward model and reference models for crust and lithosphere, it will include errors. We assume

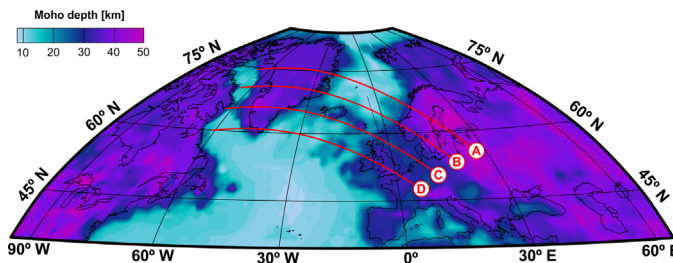


**Fig. 9.** Moho depth and locations of four lithospheric cross sections (A–D).

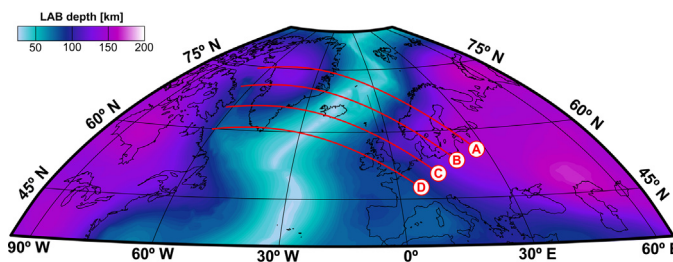


**Fig. 10.** LAB depth and locations of four lithospheric cross sections (A–D).

that by modelling sub-lithospheric pressure to optimise the calculated stress field in comparison with the WSM, we are able to retrieve a realistic image of dynamic topography variations as part of the residual topography.

As a further refinement in the NAR, more localised pressure anomalies of amplitudes  $-10$ ,  $-5$ ,  $5$  and  $10$  MPa were superimposed on the globally determined pressure model beneath the East Greenland margin, Iceland, the Scandinavian Caledonides and the Baltic Shield. Small adjustments of up to  $10$  MPa (and  $<500$  m of topographic response) are well within the error of the residual topography and, hence, we believe that this additional modelling step is valid. This was combined with local LAB depth variations of amplitudes of  $-20$ ,  $-10$ ,  $10$  and  $20$  km in order to reduce further local stress misfits in the NAR. These local adjustments beneath the Norwegian margin, the Baltic Shield and the North Sea were able to considerably improve the agreement between the modelled stress directions and the WSM observations (see Section 5.1).

The global model of both lithospheric thickness and mantle pressure was entirely based on a set of starting models that derived from observed residual topography, which were iteratively combined and averaged according to their respective fit in defined regions and thereby optimised. Poorly-fitting models were rejected; well-fitting models were retained, while new models were produced by combining and averaging the accepted models. Finally, the North Atlantic was targeted with similar local iterative optimisations.

During the iterative optimisation procedure the LAB depth model was changed with an average of approx.  $18$  km ( $15\%$ ) and the crustal thickness with approx.  $340$  m ( $2.8\%$ ). The topography was with a global average error of  $2$  m ( $0.08\%$ ) excellently recovered and the surface heat flow shows an average misfit of  $10.3$  mW/m $^2$  ( $14.4\%$ ), which is well within the global uncertainty.

It was important to retain a relatively abrupt LAB depth gradient at the continent-ocean-boundary to explain the overall stress field at passive margins. Uncertainty in the exact COB location can, however, explain rather large isostatic errors and misfits in the stress field. In case of Europe and Greenland these misfits could almost be entirely eliminated.

#### 4.5. The World Stress Map

The World Stress Map (WSM) was used as a direct validation of the LAB and pressure models. The WSM, therefore, is an observation which contributed to constraining the lithospheric and upper mantle structure by comparison with the computed stress field. The WSM suffers from an uneven distribution of observations. Some land areas like the Alps have a high density of observations, whereas vast oceanic regions and remote areas in Greenland and the Arctic are lacking data. In order to facilitate the comparison between model results and observations, the WSM observations were transferred to the model grid points using averaging disks of radii from  $50$  km to  $250$  km at every grid point. The value assigned to a grid point was the average of all stress azimuths within the disk, weighted with the inverse distance from the centre. This gave a rather local ( $<50$  km) average in regions of high data density, whereas the stress field measurements could in principle be extrapolated up to a distance of  $250$  km in regions without many data points. The average value was only accepted if at least  $3$  stress measurements were available in the current disk and if the standard deviation of the WSM observation was less than  $30^\circ$ . Many grid points will, therefore, be without interpolated WSM values. This approach was similar to the method presented in Heidbach et al. (2010). The difference to the approach by Lithgow-Bertelloni and Gwynn (2004) is the allowed uncertainty of the averaged stress azimuths and the choice of averaging in disks with different radii.

## 5. Results

The predicted maximum horizontal stress directions were quantitatively compared to the WSM. The study area was defined from  $50$  to  $85^\circ$  N and  $45^\circ$  W to  $45^\circ$  E. The initial global LAB depth adjustments were able to improve the misfit of the computed stress field from  $40.06^\circ$  to  $36.57^\circ$  (from  $25.05^\circ$  to  $23.32^\circ$  in the North Atlantic region) and the residual topography from  $1006$  m to  $646$  m. The global sub-lithospheric pressure adjustments improved the stress field further to a global average of  $36.40^\circ$  ( $22.47^\circ$  in the North Atlantic) and the residual topography down to an average of  $568$  m.

Different pressure models were tested for the North Atlantic region. Special focus was on additional positive and negative pressure anomalies beneath the Greenland Caledonides, Iceland, the Scandinavian Caledonides and the Baltic Shield. The model clearly preferred a significant pressure difference between the North Atlantic and the Scandinavian Caledonides. These small-scale adjustments further reduced the misfit between calculated and observed stress directions from  $22.47^\circ$  to  $21.58^\circ$  misfit. Similar local adjustments of the LAB depth model further decreased the misfit to  $20.71^\circ$ . Since the small scale adjustments in the North Atlantic region were not based on the residual topography but utilised the residual topography uncertainty, a slightly higher topographic misfit results as compared to the global models.

Our modelling procedure resulted in the best fitting and our preferred model. The modelling procedure seems to be very robust, with the first iteration outlining the general shape and amplitude of the anomalies and the ensuing iterations contributing some minor local complexity.

Considering the starting models, we believe that the parameter space was realistically and sufficiently defined, including both a wide spectrum of different wavelengths and different amplitudes. Thus, models with higher amplitudes and shorter wavelengths were systematically producing a larger misfit, while higher amplitudes and higher cut-off degrees of the harmonical models produced better models, both for LAB and pressure models.

### 5.1. Stress field

The computed geopotential stress field in the NAR ([Figs. 6 and 7](#)) is in very good agreement with the WSM ([Fig. 7, red](#)). Generally, the maximum horizontal stress direction is well aligned with observations in the entire study area. Contrary to this a large misfit exists in Southern Europe, focussed along the Alpine fold belt. Here, the plate boundary forces, which we do not consider, overprint the geopotential stress field and cause the misfit, as also discussed by ([Nielsen et al., 2014](#)).

The maximum deviatoric horizontal stresses are aligned with the axes of the mid ocean ridges, which are under extension perpendicular to the spreading axis. The Azores triple junction is clearly

visible in the stress field, although some observed complexity could not be recovered. The Iceland melt anomaly causes a disturbance of the North Atlantic rift axis in the direction of the Greenland-Scotland-Ridge. The deep ocean basins are under compression with the most compressive stress directions generally pointing towards the corresponding rift axis. Europe experiences generally NNW-SSE directed compressive deviatoric stresses, caused by the high geopotential energy in the Alpine fold belt and the high geopotential energy along the Mid Atlantic Ridge system. Scandinavia shows a similar tendency, while the stress field is aligned in a NWW-SEE direction along the Norwegian margin, responding to the North Atlantic ridge push and the topography of the Scandinavian Caledonides. In the northern North Sea the stress field shows a distinct

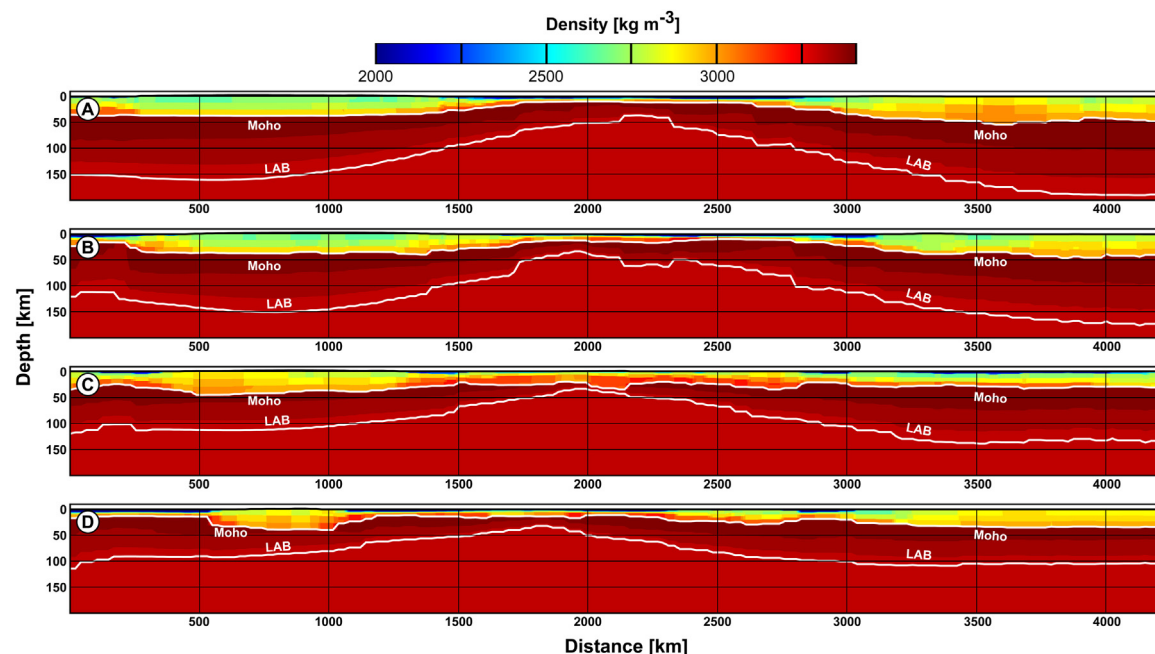


**Fig. 11.** Lithospheric density cross sections.

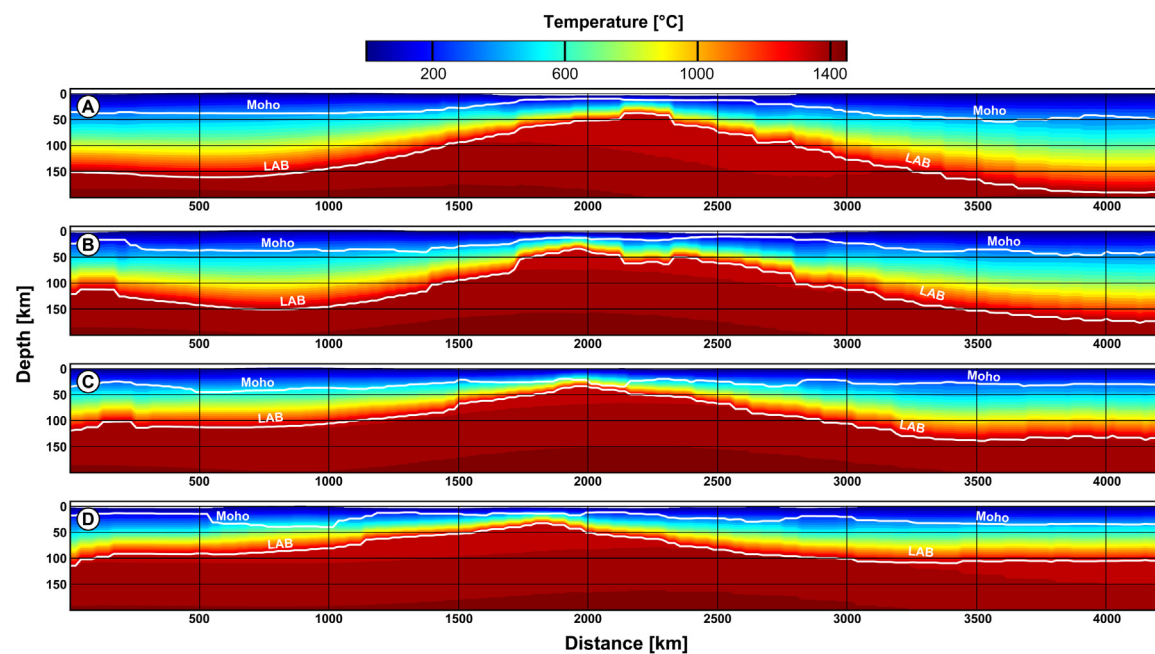


**Fig. 12.** Lithospheric temperature cross sections.

departure from this elsewhere consistent stress field in W-E direction (Pascal and Cloetingh, 2009). East Greenland shows mainly coast parallel stresses. Only further inland of the coastal ranges, the stress field in Greenland turns back to a NNW-SSE direction in the north and more NW-SE direction in the south, reflecting the high topography in East Greenland. Some continental margins show areas of misfit, especially the northern Labrador margin and the Newfoundland margin as well as the western Barents Sea margin. This might be attributed to uncertainty in the crustal and lithospheric structure, and especially the position of the COB. In Central Europe a larger region of misfit is observed in the south-eastern Polish Basin directly north of the Carpathians and the Pannonian Basin. The different orientation of the stress field here might also be related to uncertainty in structure of the basin, but probably also the vicinity to an active plate boundary (e.g. Jarosiński, 1998).

Two areas of specifically large deviation between predictions and observations (Fig. 8A and B) are identified in the northern North Sea (A) and in Central Scandinavia (B). Here, the same potential reasons for this deviation might be valid: tectonic activity or an insufficient geopotential energy model as a consequence of a wrong lithospheric density model or sub-lithospheric pressure. Area A is situated within the most active seismic zones in the region, south of the Møre Trøndelag Fault Complex (MTFC), the Great Glen Fault (GGF) and the Walls Boundary Fault (WBF). Numerical modelling of this complex setting shows a similar pattern of perturbations in the stress field (Pascal and Gabrielsen, 2001). The sedimentary, crustal and lithospheric structure can be assumed to be complex in the area and possibly not resolved by the model. A wrong sub-lithospheric pressure cannot be ruled out. Finally, an additional overprint of the stress field might come from post-glacial uplift; however, the exact tectonic impact is discussed (Wu et al., 1999; Bungum et al., 2010). We, therefore, suggest that it is highly likely that this fault system is responsible for the regional stress field perturbation, but probably the superimposition of several sources for the stress field perturbation. Area B in Central Scandinavia is far away from any active faults and seismicity why a tectonically caused stress misfit is unlikely. The area is, however, located in the centre of the area affected by post-glacial rebound (Fig. 8, red stippled line). We suggest that the misfit in area B is at least partly caused by effects from post-glacial uplift, possibly enhanced by uncertainties in the lithospheric and crustal structure in the western margin of the East European Craton.

## 5.2. Lithospheric and sub-lithospheric pressure model

The global optimisation approach required some changes in crustal structure (Fig. 9) and LAB depth (Fig. 10). Some physical quantities used in the lithospheric forward model are poorly constrained and literature values were chosen to describe thermal conductivity, thermal expansion coefficient and heat production. Also the reference densities of the incorporated layers are probably poorly constrained. We will, therefore, not evaluate any minor changes in these parameters. Moho depth and LAB depth, however, can be compared with observations. The LAB depth was changed by on average approx. 18 km (15%) and the crustal thickness by approx. 340 m (2.8%), which is well within the resolution of observations. Worth mentioning is that it was essential to retain a relatively abrupt LAB gradient at the COB. A locally thicker lithosphere beneath the Vøring margin and the North Sea was also required to improve the stress field, whereas the Jan Mayen area required a thinner lithospheric thickness as compared to other continental areas. Four cross sections of the lithosphere density and thermal structure are shown in Figs. 11 and 12, respectively.

The sub-lithospheric pressure anomaly in the NAR (Fig. 13) shows a distinct localised anomaly that peaks beneath Iceland with ~25 MPa and terminates at the very south-eastern margin of East Greenland, the Faroe Islands and Jan Mayen. A similar but much less

expressed pressure anomaly with a maximum of 15 MPa is located beneath the Azores triple junction. The continents seem to be much less influenced by pressure anomalies; however, North America and Greenland mostly show positive pressure of up to 10 MPa, whereas Europe shows much lower pressure, with anomalies down to -10 MPa.

In the dynamic topography model for the North Atlantic (Fig. 14), corresponding to the final sub-lithospheric pressure anomaly (Fig. 13), the Iceland melt anomaly stands out as an area of significant dynamic support of circa 1000 m, weakly connected to the Azores melt anomaly with circa 600 m of support and decreasing with distance. The North Atlantic conjugate margins seem to be affected quite differently by this dynamic support. Along the European continental margin, the dynamic topography increases smoothly from a minimum of c. -70 m in northern, ~100 m in southern Norway to circa 300 m in northern Scotland. The East Greenland margin shows more robust dynamic support of 250–350 m. This includes the King Oscar Fjord area, the Central Fjord System, and significant support prevails until south of Danmarkshavn.

## 6. Discussion

Iterative modelling of the sub-lithospheric pressure in the North Atlantic regions revealed a distinct pattern that results in a superior fit of the observed stresses in the region. This pressure shows low amplitudes beneath Norway and slightly higher beneath the easternmost margin of Greenland and the northern cost of Britain with a clear peak under Iceland. Other models, including higher pressures in Scandinavia and/or lower pressure beneath Iceland were rejected by the modelling. The global misfit of 36.54° of the final stress model is comparable to previously published models, which used more sophisticated computations including more sources of stress. For example, Steinberger et al. (2001) obtained a global misfit of 30.37–31.19° and Lithgow-Bertelloni and Guynn (2004) obtained 32° for the best model. The misfit of 20.71° in the North Atlantic lies probably just above the uncertainty of the WSM, which is estimated to be 10–15° for the best and more than 25° for the weakest contributing observations (Lithgow-Bertelloni and Guynn, 2004). Given the good agreement of modelled and observed stress directions, we believe that our dynamic topography and mantle pressure model of the NAR echoes a realistic snapshot of the present-day situation.

### 6.1. Error sources and robustness

The present modelling approach relies on starting models of crustal and lithospheric structure, the World Stress Map and the interpolation to the model grid, assumptions on the rheological and elastic properties (e.g. constant thickness of the elastic lithosphere) and approximations in the stress equations (e.g. no sub-lithospheric basal drag). The question is whether these choices were realistic and how much uncertainty might be produced by this approach. We avoided incorporating less well-constrained quantities, which may have added additional uncertainty. For instance, we neglected laterally varying elastic thickness, mantle viscosity or sub-lithospheric basal stresses derived from mantle convection patters. Clearly, these quantities do have an effect on the stress field, but are not trivial to quantify and matter of research and discussion (Lithgow-Bertelloni and Guynn, 2004; Naliboff et al., 2009; Höink et al., 2011; Ghosh and Holt, 2012). The WSM and the averaged data set probably has an uncertainty of 15–20°, which is quite large considering the ranges of misfit we are dealing with (<35°). Given this, the best fitting model as presented in Figs. 13 and 14, which we believe

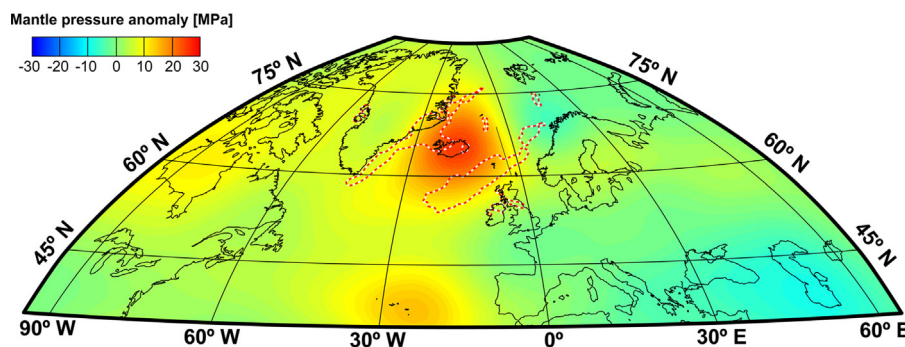


**Fig. 13.** Final optimised mantle pressure anomaly in the NAR and the outline of Palaeocene-early Eocene break-up related magmatic products (red-white).

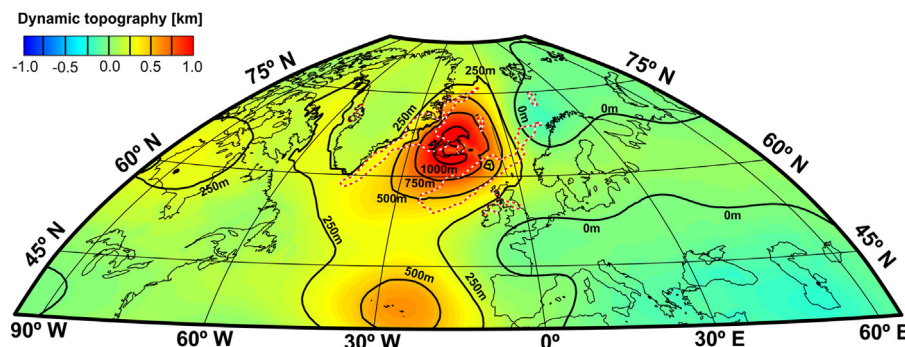


**Fig. 14.** Dynamic topography in the NAR, according to the final, optimised lithospheric and pressure model and assuming local isostasy and the outline of Palaeocene-early Eocene break-up related magmatic products (red-white).

to be realistic and representative, may be bestowed with uncertainty.

We aim to quantify the variation of the modelled quantities by assessing the mean and the standard deviation of all tested models. This may provide a representative estimate of the variation, uncertainty and robustness of the models (Fig. 15). The regional pattern of pressure and dynamic topography appears to be robust. The fact that we only model stress directions and not absolute values of stress amplitude implies that the pressure amplitude may be variable as well, while obtaining the same stress directions, because the pressure gradients are still retained. This is generally correct, but slightly more complicated, since the stress field, in fact, depends on the relative contribution of both the lithosphere and sub-lithospheric pressure, although the clear weight in the modelling is on the latter. Iceland shows a range from 750 to 1000 m peak dynamic uplift and the Azores 500–750 m. Dynamic support in northern Norway has a range between 0 and 200 m and southern Norway between 100 and 350 m. The northernmost tip of Britain and the Scoresby Sund area show the most substantial support in the continental areas with 250 and 750 m. Central East Greenland ranges between 250 and 500 m.

We are confident that the large scale picture obtained in this study is valid. We expect that the most realistic model lies somewhere within the model variation (mean  $\pm$  standard deviation) and that the obtained regional gradients are the most robust feature. The absolute amplitude, however, might be absolutely shifted or relatively scaled. The here presented best fitting models were obviously limited by the chosen parameter space (amplitude and wavelengths). Our modelling approach is straight-forward and provides a best model and a rough estimate of model uncertainty, within the predefined parameter space. Compared to many other approaches, which rather test a number of deterministic model realisations of mantle convection patterns, elastic thicknesses or

pressure, we believe that our approach represents a valid and robust modelling scheme.

## 6.2. Geodynamic implications

Our snapshot model of the present day does not connect directly to the North Atlantic evolution since continental break up at c. 56 Ma. We will, however, derive some literature backed inferences regarding the vertical motions in the NAR during the last approx. 60 Ma.

Dynamic topography can in general be assumed not to exceed some hundreds of meters and to be of large wavelength (Braun, 2010; Molnar et al., 2015). Furthermore, lithospheric modifications, delamination and deformation are unlikely in Central East Greenland, since a basically intact fossil subduction zone is preserved within the lithospheric mantle to depths of 120 km (Schiffer et al., 2014, 2015a). Iceland, clearly exceeding a dynamic uplift of several hundreds of meters, forms a special case related to the still active anomalous melt production. Despite the clear presence of an upper mantle anomaly, large uncertainty in crustal (and upper mantle) composition and structure and the transition to the upper mantle (Gudmundsson, 2003) as well as possibly inherited continental fragments (Fedorova et al., 2005; Foulger, 2006) complicate the isostatic assessment of Iceland and thereby that of residual topography and dynamic support. The large dynamic uplift around Iceland might, therefore, contain a contribution from an erroneous crustal model.

Based on reliable dating and explicit evidence of subaerial processes there is general consensus that many of the flood basalt regions in the NAR were subaerial during rifting (Ziegler, 1990; Larsen and Saunders, 1998; Torsvik et al., 2002; MacLennan and Jones, 2006). This includes the Voring margin (Skogseid et al., 1992, 2000; Skogseid, 1994; Roberts et al., 1997; Ren et al., 2003), Hatton Bank, Rockall Plateau (Stoker et al., 2012) and the Faroe-Shetland

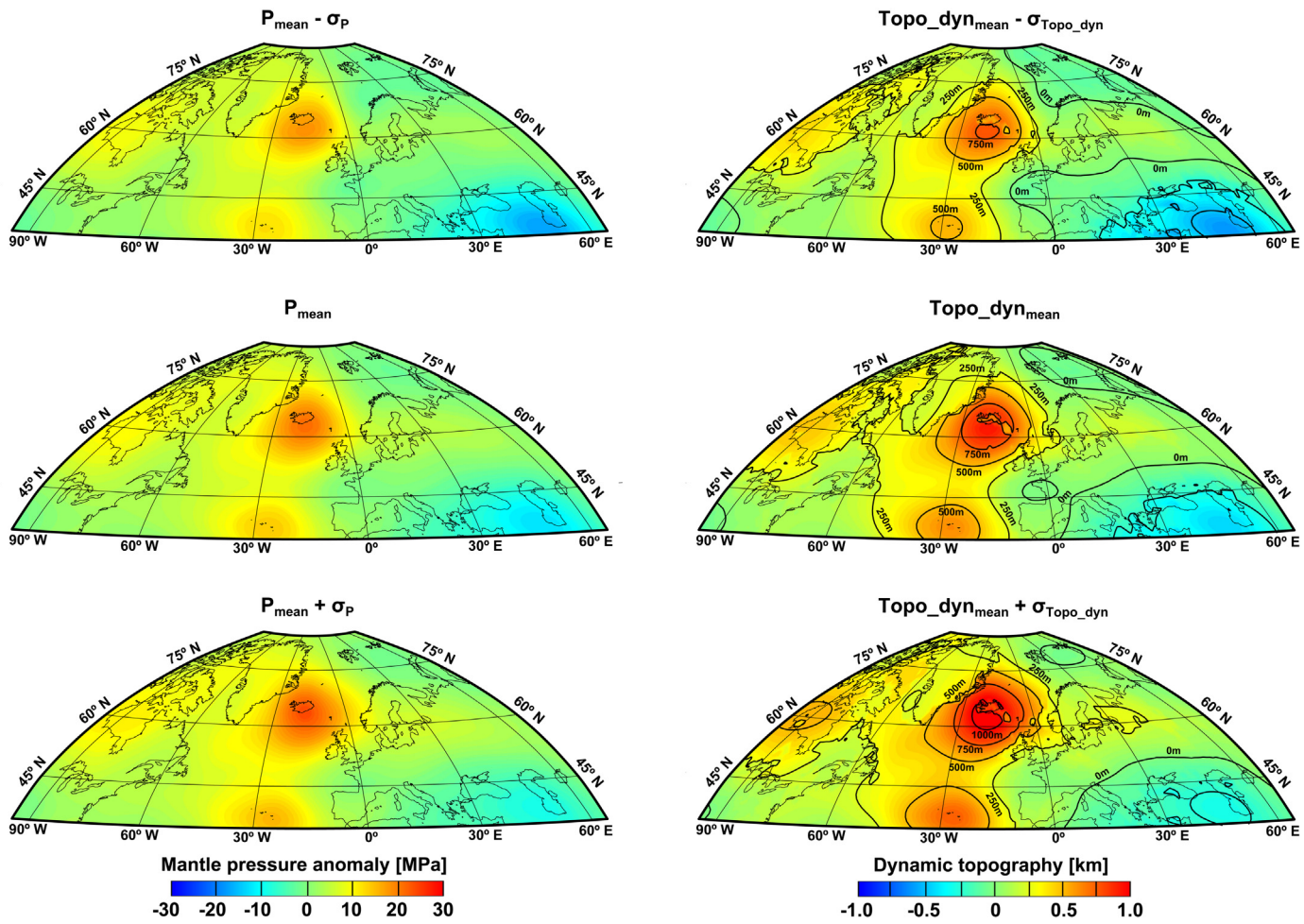


**Fig. 15.** The average (middle panel) of all tested pressure (left) and dynamic topography models (right) and the lower and the lower and upper limit of the 90% confidentiality of all models (upper and lower panel, respectively). All models as well as the lower bound and upper bound show a similar pattern, with a clear positive maximum surrounding Iceland. Although these are not the best fitting models, these illustrate that the general interpretation of the best fitting model are still valid for the end-member models.

platform (Tassone et al., 2014). The subaerial basalts of the Faeroe Islands overly marine sediments of Cretaceous age (Fliedner and White, 2003; Fletcher et al., 2013) and are interbedded with coals with subaerial micro-fauna (Lund, 1989).

Vitrinite reflectance ( $R_o$ ) of middle Jurassic bituminous coals in western Germania Land in the range 0.49–0.53% (Bojesen-Koefoed et al., 2012) and in Hochstetter Forland and Kuhn Ø ( $R_o$  suppressed) c. 0.30% indicate a previous deeper burial of the present surface of East Greenland. However, the timing of the exhumation of the surface is not known. East and West Greenland (Medvedev et al., 2008; Medvedev et al., 2013) and Scandinavia (Gołędowski et al., 2013; Medvedev and Hartz, 2015) have experienced deep glacial erosion of fjords and also of the intervening flattish areas with an ensuing km-scale flexural uplift of the rock column as a consequence. Similar erosion rates are estimated for western Germania land–Northeast Greenland (Pedersen et al., 2013).

Our analysis corroborates the inference that present-day dynamic uplift in excess of 350 m in East Greenland is very unlikely (cf. Schiffer et al., 2015b), which is why the alleged Neogene pulse of km-scale uplift in East Greenland and its postulated role in preconditioning Greenland's glaciation remains controversial (Steinberger et al., 2015 and references therein).

The evidence that many areas along the North Atlantic rift system, especially along the Norwegian margin, have been sub-aerial before and during break-up and are several hundred meters beneath sea-level at present day obviously implies that many of

these regions have experienced subsidence—some areas more than others. East Greenland, the Faroe Islands, northern Britain and Iceland are examples where flood basalts are still sub-aerial. The exact timing of the vertical motions during the last ~60 Myr cannot be constrained by our approach.

In view of the subsidence of previously subaerial areas the magmatic activity dissipated relatively quickly after breakup (Larsen and Tegner, 2006; Brown and Lesher, 2014) until it almost entirely diminished at ~35 Ma (Storey et al., 2007), and remained almost exclusively along the MOR and Iceland (Holbrook et al., 2001).

## 7. Conclusion

We have presented an iterative modelling approach to assess the sub-lithospheric pressure globally and locally for the North Atlantic. In the process, part of the topography was explained by adjusting the lithospheric thickness. Calculation of the stress field resulting from the gradients of the potential energy allowed the use of the WSM as an observable to test the pressure and lithospheric model. The modelling procedure focussed on the NAR with additional optimisation iterations. The resulting potential energy and stress model agrees very well with the WSM observations.

The WSM data and the crustal and LAB models prefer a sub-lithospheric pressure model that causes negligible dynamic uplift (<150 m amplitude) in Scandinavia, whereas the East Greenland margin and northern Britain show a slightly larger dynamic uplift

(250–350 m), which clearly is related to the main pressure anomaly beneath Iceland of diameter 1200–1800 km.

The stress validated pressure and associated dynamic topography model further allowed us to discuss the transient and spatial character of the Iceland melt anomaly since its formation. Whereas the Norwegian margin must have experienced a an almost entire decrease in dynamic support since early Cenozoic, central East Greenland and northernmost Scotland are still supported by an unknown fraction of the initial amplitude of dynamic support. Also the Faroe Islands still exhibit considerable dynamic support from a mantle anomaly, clearly related to the Iceland melt anomaly.

Our results support the impingement of a large scale buoyancy anomaly on the base of the lithosphere and the relatively rapid dissipation of the fringes of this anomaly. The exact sources for this buoyancy anomaly cannot be identified in this study but the overall picture does neither exclude a mantle plume, nor any other potential mechanisms. This in turn points to a relatively simple topography evolution: transient and more durable uplift was installed during the Palaeocene-Eocene, followed by relaxation of the transient uplift component, whereas a more durable anomaly established in the closest vicinity of Iceland.

## Acknowledgements

This paper was produced under the umbrella of the project “Topography of the North Atlantic Realm” (TOPOREAL), financed by The Danish Council for Independent Research (DFF). We thank DFF and all actively involved participants of TOPOREAL and all others who contributed to the discussion of the results. This paper was finalised as part of C. Schiffer’s postdoctoral fellowship at Durham University supported by the Carlsberg Foundation. We thank the reviewers (Christophe Pascal and Giampiero Iaffaldano and two anonymous) for very constructive and helpful comments.

## References

- Andersen, T.B., Jamtveit, B., Dewey, J.F., Swensson, E., 1991. Subduction and eduction of continental crust: major mechanisms during continent–continent collision and orogenic extensional collapse, a model based on the south Norwegian Caledonides. *Terra Nova* 3 (3), 303–310, <http://dx.doi.org/10.1111/j.1365-3121.1991.tb00148.x>.
- Anderson, D.L., 2001. Top-down tectonics? *Science* 293 (5537), 2016–2018, <http://dx.doi.org/10.1126/science.1065448>.
- Anell, I., Thybo, H., Artemieva, I.M., 2009. Cenozoic uplift and subsidence in the North Atlantic region: geological evidence revisited. *Tectonophysics* 474 (1–2), 78–105, <http://dx.doi.org/10.1016/j.tecto.2009.04.006>.
- Artemieva, I.M., 2009. The continental lithosphere: reconciling thermal, seismic, and petrologic data. *Lithos* 109, 23–46, <http://dx.doi.org/10.1016/j.lithos.2008.09.015>.
- Artemieva, I.M., Thybo, H., 2013. EUNAseis: a seismic model for Moho and crustal structure in Europe/Greenland, and the North Atlantic region. *Tectonophysics* 609, 97–153, <http://dx.doi.org/10.1016/j.tecto.2013.08.004>.
- Artemieva, I.M., Thybo, H., Kaban, M.K., 2006. Deep Europe today: geophysical synthesis of the upper mantle structure and lithospheric processes over 3.5 Ga. *Geological Society, London Memoirs* 32 (1), 11–41, <http://dx.doi.org/10.1144/GSL.MEM.2006.032.01.02>.
- Balling, N., 1980. The land uplift in Fennoscandia, gravity field anomalies and isostasy. In: Mörner, N.-A. (Ed.), *Earth Rheology, Isostasy and Eustasy*. John Wiley & Sons, New York, pp. 297–321.
- Bird, P., Piper, K., 1980. Plane-stress finite-element models of tectonic flow in southern California. *Phys. Earth Planet. Inter.* 21 (2–3), 158–175, [http://dx.doi.org/10.1016/0031-9201\(80\)90067-9](http://dx.doi.org/10.1016/0031-9201(80)90067-9).
- Bird, P., Liu, Z., Rucker, W.K., 2008. Stresses that drive the plates from below: definitions, computational path, model optimization, and error analysis. *J. Geophys. Res.* 113, B11406, <http://dx.doi.org/10.1029/2007jb005460>.
- Bojesen-Koefoed, J.A., Kalkreuth, W., Petersen, H.I., Piasecki, S., 2012. A remote coal deposit revisited: middle Jurassic coals at Kulhej, western Germania Land, northeast Greenland. *Int. J. Coal Geol.* 98, 50–61, <http://dx.doi.org/10.1016/j.coal.2012.04.006>.
- Bonow, J.M., Japsen, P., Nielsen, T.F.D., 2014. High-level landscapes along the margin of southern East Greenland—a record of tectonic uplift and incision after breakup in the NE Atlantic. *Global Planet. Change* 116, 10–29, <http://dx.doi.org/10.1016/j.gloplacha.2014.01.010>.
- Bott, M., 1991. Ridge push and associated plate interior stress in normal and hot-spot regions. *Tectonophysics* 200 (1–3), 17–32, [http://dx.doi.org/10.1016/0040-1951\(91\)90003-b](http://dx.doi.org/10.1016/0040-1951(91)90003-b).
- Bouhifd, M.A., Andrault, D., Fiquet, G., Richet, P., 1996. Thermal expansion of forsterite up to the melting point. *Geophys. Res. Lett.* 23 (10), 1143–1146, <http://dx.doi.org/10.1029/96GL01118>.
- Braun, A., Kim, H.R., Csatho, B., von Frese, R.R.B., 2007. Gravity-inferred crustal thickness of Greenland. *Earth Planet. Sci. Lett.* 262 (1–2), 138–158, <http://dx.doi.org/10.1016/j.epsl.2007.07.050>.
- Braun, J., 2010. The many surface expressions of mantle dynamics. *Nat. Geosci.* 3 (12), 825–833, <http://dx.doi.org/10.1038/ngeo1020>.
- Brown, E.L., Lesser, C.E., 2014. North Atlantic magmatism controlled by temperature, mantle composition and buoyancy. *Nat. Geosci.* 7 (11), 820–824, <http://dx.doi.org/10.1038/ngeo2264>.
- Bungum, H., Olesen, O., Pascal, C., Gibbons, S., Lindholm, C., VestØl, O., 2010. To what extent is the present seismicity of Norway driven by post-glacial rebound? *J. Geol. Soc.* 167 (2), 373–384, <http://dx.doi.org/10.1144/0016-76492009-009>.
- Cammarano, F., Goes, S., Vacher, P., Giardini, D., 2003. Inferring upper-mantle temperatures from seismic velocities. *Phys. Earth Planet. Inter.* 138 (3–4), 197–222, [http://dx.doi.org/10.1016/s0031-9201\(03\)00156-0](http://dx.doi.org/10.1016/s0031-9201(03)00156-0).
- Chalmers, J.A., Green, P., Japsen, P., Rasmussen, E.S., 2010. The Scandinavian mountains have not persisted since the Caledonian orogeny. A comment on Nielsen et al (2009a). *J. Geodyn.* 50 (2), 94–101, <http://dx.doi.org/10.1016/j.jog.2010.02.001>.
- Conrad, C.P., Lithgow-Bertelloni, C., 2006. Influence of continental roots and asthenosphere on plate-mantle coupling. *Geophys. Res. Lett.* 33 (5), L05312, <http://dx.doi.org/10.1029/2005gl025621>.
- Conrad, C.P., Lithgow-Bertelloni, C., Louden, K.E., 2004. Iceland, the Farallon slab, and dynamic topography of the North Atlantic. *Geology* 32 (3), 177–180, <http://dx.doi.org/10.1130/G20137.1>.
- Dahl-Jensen, T., Larsen, T.B., Woelbern, I., Bach, T., Hanka, W., Kind, R., Gregersen, S., Mosegaard, K., Voss, P., Gudmundsson, O., 2003. Depth to Moho in Greenland: receiver-function analysis suggests two Proterozoic blocks in Greenland. *Earth Planet. Sci. Lett.* 205 (3–4), 379–393, [http://dx.doi.org/10.1016/s0012-821x\(02\)01080-4](http://dx.doi.org/10.1016/s0012-821x(02)01080-4).
- Darbyshire, F.A., Priestley, K.F., White, R.S., Stefánsson, R., Gudmundsson, G.B., Jakobsdóttir, S.S., 2000. Crustal structure of central and northern Iceland from analysis of teleseismic receiver functions. *Geophys. J. Int.* 143 (1), 163–184, <http://dx.doi.org/10.1046/j.1365-246X.2000.00224.x>.
- Darbyshire, F.A., Larsen, T.B., Mosegaard, K., Dahl-Jensen, T., Gudmundsson, Ó., Bach, T., Gregersen, S., Pedersen, H.A., Hanka, W., 2004. A first detailed look at the Greenland lithosphere and upper mantle, using Rayleigh wave tomography. *Geophys. J. Int.* 158 (1), 267–286, <http://dx.doi.org/10.1111/j.1365-246X.2004.02316.x>.
- Dewey, J.F., Ryan, P.D., Andersen, T.B., 1993. Orogenic uplift and collapse, crustal thickness, fabrics and metamorphic phase changes: the role of eclogites. *Geol. Soc. Lond. Special Publ.* 76 (1), 325–343, <http://dx.doi.org/10.1144/GSL.SP.1993.076.01.16>.
- Ebbing, J., England, R.W., Korja, T., Lauritsen, T., Olesen, O., Stratford, W., Weidle, C., 2012. Structure of the Scandes lithosphere from surface to depth. *Tectonophysics* 536–537, 1–24, <http://dx.doi.org/10.1016/j.tecto.2012.02.016>.
- Egholm, D.L., Nielsen, S.B., Pedersen, V.K., Lesemann, J.-E., 2009. Glacial effects limiting mountain height. *Nature* 460 (7257), 884–887, <http://dx.doi.org/10.1038/nature08263>.
- England, P., Houseman, G., 1986. Finite strain calculations of continental deformation: 2. Comparison with the India-Asia Collision Zone. *J. Geophys. Res.: Solid Earth* 91, 3664–3676, <http://dx.doi.org/10.1029/JB091iB03p03664>.
- England, P., McKenzie, D., 1982. A thin viscous sheet model for continental deformation. *Geophys. J. R. Astron. Soc.* 70 (2), 295–321, <http://dx.doi.org/10.1111/j.1365-246X.1982.tb04969.x>.
- Fedorova, T., Jacoby, W.R., Wallner, H., 2005. Crust-mantle transition and Moho model for Iceland and surroundings from seismic, topography, and gravity data. *Tectonophysics* 396 (3–4), 119–140, <http://dx.doi.org/10.1016/j.tecto.2004.11.004>.
- Fichler, C., Odinsen, T., Rueslätten, H., Olesen, O., Vindstad, J.E., Wienecke, S., 2011. Crustal inhomogeneities in the Northern North Sea from potential field modeling: inherited structure and serpentinites? *Tectonophysics* 510 (1–2), 172–185, <http://dx.doi.org/10.1016/j.tecto.2011.06.026>.
- Fischer, K.M., Ford, H.A., Abt, D.L., Rychert, C.A., 2010. The lithosphere–asthenosphere boundary. *Annu. Rev. Earth Planet. Sci.* 38 (1), 551–575, <http://dx.doi.org/10.1146/annurev-earth-040809-152438>.
- Fittion, J.C., Saunders, A.D., Norry, M.J., Hardarson, B.S., Taylor, R.N., 1997. Thermal and chemical structure of the Iceland plume. *Earth Planet. Sci. Lett.* 153 (3–4), 197–208, [http://dx.doi.org/10.1016/s0012-821x\(97\)00170-2](http://dx.doi.org/10.1016/s0012-821x(97)00170-2).
- Flament, N., Gurnis, M., Müller, R.D., 2013. A review of observations and models of dynamic topography. *Lithosphere*, 5, L245.1, <http://dx.doi.org/10.1130/L245.1>.
- Flesch, L.M., Kreemer, C., 2010. Gravitational potential energy and regional stress and strain rate fields for continental plateaus: examples from the central Andes and Colorado Plateau. *Tectonophysics* 482 (1–4), 182–192, <http://dx.doi.org/10.1016/j.tecto.2009.07.014>.
- Flesch, L.M., Haines, A.J., Holt, W.E., 2001. Dynamics of the India-Eurasia collision zone. *J. Geophys. Res.: Solid Earth* 106 (B8), 16435–16460, <http://dx.doi.org/10.1029/2001jb000208>.

- Fletcher, R., Kusznir, N., Roberts, A., Hunsdale, R., 2013. The formation of a failed continental breakup basin: the Cenozoic development of the Faroe-Shetland Basin. *Basin Res.* 25 (5), 532–553, <http://dx.doi.org/10.1111/bre.12015>.
- Fliedner, M.M., White, R.S., 2003. Depth imaging of basalt flows in the Faeroe-Shetland Basin. *Geophys. J. Int.* 152 (2), 353–371, <http://dx.doi.org/10.1046/j.1365-246X.2003.01833.x>.
- Fossen, H., 2010. Extensional tectonics in the North Atlantic Caledonides: a regional view. *Geol. Soc. Lond. Special Publ.* 335 (1), 767–793, <http://dx.doi.org/10.1144/SP335.31>.
- Foulger, G.R., Pritchard, M.J., Julian, B.R., Evans, J.R., Allen, R.M., Nolet, G., Morgan, W.J., Bergsson, B.H., Erlendsson, P., Jakobsdóttir, S., Ragnarsson, S., Stefansson, R., Vogfjörd, K., 2000. The seismic anomaly beneath Iceland extends down to the mantle transition zone and no deeper. *Geophys. J. Int.* 142 (3), F1–F5, <http://dx.doi.org/10.1046/j.1365-246X.2000.00245.x>.
- Foulger, G.R., Pritchard, M.J., Julian, B.R., Evans, J.R., Allen, R.M., Nolet, G., Morgan, W.J., Bergsson, B.H., Erlendsson, P., Jakobsdóttir, S., Ragnarsson, S., Stefansson, R., Vogfjörd, K., 2001. Seismic tomography shows that upwelling beneath Iceland is confined to the upper mantle. *Geophys. J. Int.* 146 (2), 504–530, <http://dx.doi.org/10.1046/j.0956-540x.2001.01470.x>.
- Foulger, G.R., Du, Z., Julian, B.R., 2003. Icelandic-type crust. *Geophys. J. Int.* 155 (2), 567–590, <http://dx.doi.org/10.1046/j.1365-246X.2003.02056.x>.
- Foulger, G.R., Natland, J.H., Anderson, D.L., 2005. A source for Icelandic magmas in remelted Iapetus crust. *J. Volcanol. Geotherm. Res.* 141 (1–2), 23–44, <http://dx.doi.org/10.1016/j.jvolgeores.2004.10.006>.
- Foulger, G.R., Panza, G.F., Artemieva, I.M., Bastow, I.D., Cammarano, F., Evans, J.R., Hamilton, W.B., Julian, B.R., Lustrino, M., Thybo, H., Yanovskaya, T.B., 2013. Caveats on tomographic images. *Terra Nova* 25 (4), 259–281, <http://dx.doi.org/10.1111/ter.12041>.
- Foulger, G., Panza, G., Artemieva, I., Bastow, I., Cammarano, F., Doglioni, C., Evans, J., Hamilton, W., Julian, B., Lustrino, M., Thybo, H., Yanovskaya, T., 2015. What lies deep in the mantle below? *Eos* 96, <http://dx.doi.org/10.1029/2015EO034319>.
- Foulger, G.R., 2006. Older crust underlies Iceland. *Geophys. J. Int.* 165 (2), 672–676, <http://dx.doi.org/10.1111/j.1365-246X.2006.02941.x>.
- Gölke, M., Coblenz, D., 1996. Origins of the European regional stress field. *Tectonophysics* 266 (1–4), 11–24, [http://dx.doi.org/10.1016/s0040-1951\(96\)00180-1](http://dx.doi.org/10.1016/s0040-1951(96)00180-1).
- Gee, D.G., Stephenson, R.A., 2006. The European lithosphere: an introduction. *Geol. Soc. Lond. Mem.* 32 (1), 1–9, <http://dx.doi.org/10.1144/GSL.MEM.2006.032.01.01>.
- Gee, D.G., Fossen, H., Henriksen, N., Higgins, A.K., 2008. From the early Paleozoic platforms of Baltica and Laurentia to the Caledonide orogen of Scandinavia and Greenland.  *Episodes*.
- Gernigon, L., Blischke, A., Nasuti, A., Sand, M., 2015. Conjugate volcanic rifted margins, sea-floor spreading and microcontinent: insights from new high-resolution aeromagnetic surveys in the Norway Basin. *Tectonics*, <http://dx.doi.org/10.1002/2014tc003717>, p. 2014TC003717.
- Ghosh, A., Holt, W.E., 2012. Plate motions and stresses from global dynamic models. *Science* 335 (6070), 838–843, <http://dx.doi.org/10.1126/science.1214209>.
- Ghosh, A., Holt, W.E., Wen, L., Haines, A.J., Flesch, L.M., 2008. Joint modeling of lithosphere and mantle dynamics elucidating lithosphere-mantle coupling. *Geophys. Res. Lett.* 35 (16), L16309, <http://dx.doi.org/10.1029/2008gl034365>.
- Ghosh, A., Holt, W.E., Flesch, L.M., 2009. Contribution of gravitational potential energy differences to the global stress field. *Geophys. J. Int.* 179 (2), 787–812, <http://dx.doi.org/10.1111/j.1365-246X.2009.04326.x>.
- Ghosh, A., Holt, W.E., Wen, L., 2013. Predicting the lithospheric stress field and plate motions by joint modeling of lithosphere and mantle dynamics. *J. Geophys. Res.: Solid Earth* 118 (1), 346–368, <http://dx.doi.org/10.1029/2012JB009516>.
- Gilchrist, A.R., Summerfield, M.A., 1990. Differential denudation and flexural isostasy in formation of rifted-margin upwarps. *Nature* 346 (6286), 739–742, <http://dx.doi.org/10.1038/346739a0>.
- Golędowski, B., Egholm, D.L., Nielsen, S.B., Clausen, O.R., McGregor, E.D., 2013. Cenozoic erosion and flexural isostasy of Scandinavia. *J. Geodyn.* 70, 49–57, <http://dx.doi.org/10.1016/j.jog.2013.05.004>.
- Grünthal, G., Stromeier, D., 1992. The recent crustal stress field in central Europe: trajectories and finite element modeling. *J. Geophys. Res.: Solid Earth* 97 (B8), 11805–11820, <http://dx.doi.org/10.1029/91jb01963>.
- Grad, M., Tiira, T., Working Group, E.S.C., 2009. The Moho depth map of the European Plate. *Geophys. J. Int.* 176 (1), 279–292, <http://dx.doi.org/10.1111/j.1365-246X.2008.03919.x>.
- Grämann, S., Ebbing, J., Fulléa, J., 2013. Integrated geophysical modelling of a lateral transition zone in the lithospheric mantle under Norway and Sweden. *Geophys. J. Int.* 194 (3), 1358–1373, <http://dx.doi.org/10.1093/gji/ggt213>.
- Green, P.F., Lidmar-Bergström, K., Japsen, P., Bonow, J.M., Chalmers, J.A., 2013. Stratigraphic landscape analysis, thermochronology and the episodic development of elevated, passive continental margins and Greenland. *Geol. Survey Denmark Greenland Bull.* 30 (150).
- Gudmundsson, Ó., 2003. The dense root of the Iceland crust. *Earth Planet. Sci. Lett.* 206 (3–4), 427–440, [http://dx.doi.org/10.1016/s0012-821x\(02\)01110-x](http://dx.doi.org/10.1016/s0012-821x(02)01110-x).
- Gung, Y., Panning, M., Romanowicz, B., 2003. Global anisotropy and the thickness of continents. *Nature* 422 (6933), 707–711, <http://dx.doi.org/10.1038/nature01559>.
- Höink, T., Lenardic, A., 2010. Long wavelength convection Poiseuille–Couette flow in the low-viscosity asthenosphere and the strength of plate margins. *Geophys. J. Int.* 180 (1), 23–33, <http://dx.doi.org/10.1111/j.1365-246X.2009.04404.x>.
- Höink, T., Jellinek, A.M., Lenardic, A., 2011. Viscous coupling at the lithosphere–asthenosphere boundary. *Geochem. Geophys. Geosyst.* 12 (10), <http://dx.doi.org/10.1029/2011gc003698>.
- Heidbach, O., Tingay, M., Barth, A., Reinecker, J., Kurfeß, D., Müller, B., 2010. Global crustal stress pattern based on the World Stress Map database release 2008. *Tectonophysics* 482 (1–4), 3–15, <http://dx.doi.org/10.1016/j.tecto.2009.07.023>.
- Hejrani, B., Balling, N., Jacobsen, B.H., Tilmann, F., 2015. Upper-mantle P- and S-wave velocities across the Northern Tornquist Zone from traveltime tomography. *Geophys. J. Int.* 203 (1), 437–458, <http://dx.doi.org/10.1093/gji/ggv291>.
- Hier-Majumder, S., 2008. Influence of contiguity on seismic velocities of partially molten aggregates. *J. Geophys. Res.: Solid Earth* 113 (B12), B12205, <http://dx.doi.org/10.1029/2008jb005662>.
- Holbrook, W.S., Larsen, H.C., Korenaga, J., Dahl-Jensen, T., Reid, I.D., Kelemen, P.B., Hopper, J.R., Kent, G.M., Lizarralde, D., Bernstein, S., Detrick, R.S., 2001. Mantle thermal structure and active upwelling during continental breakup in the North Atlantic. *Earth Planet. Sci. Lett.* 190 (3–4), 251–266, [http://dx.doi.org/10.1016/s0012-821x\(01\)00392-2](http://dx.doi.org/10.1016/s0012-821x(01)00392-2).
- Japsen, P., Chalmers, J.A., 2000. Neogene uplift and tectonics around the North Atlantic: overview. *Global Planet. Change* 24 (3–4), 165–173, [http://dx.doi.org/10.1016/s0921-8181\(00\)00006-0](http://dx.doi.org/10.1016/s0921-8181(00)00006-0).
- Japsen, P., Green, P.F., Bonow, J.M., Rasmussen, E.S., Chalmers, J.A., Kjennerud, T., 2010. Episodic uplift and exhumation along North Atlantic passive margins: implications for hydrocarbon prospectivity. *Geol. Soc. Lond. Pet. Geol. Conf. Series* 7, 979–1004, <http://dx.doi.org/10.1144/0070979>.
- Japsen, P., Green, P.F., Chalmers, J.A., 2013. The mountains of North-East Greenland are not remnants of the Caledonian topography. A comment on Pedersen et al. (2012). *Tectonophysics* vol. 530–531, p. 318–330. *Tectonophysics* 589, 234–238, <http://dx.doi.org/10.1016/j.tecto.2012.07.026>.
- Japsen, P., Green, P.F., Bonow, J.M., Nielsen, T.F.D., Chalmers, J.A., 2014. From volcanic plains to glaciated peaks: burial, uplift and exhumation history of southern East Greenland after opening of the NE Atlantic. *Global Planet. Change* 116, 91–114, <http://dx.doi.org/10.1016/j.gloplacha.2014.01.012>.
- Jarosiński, M., Beekman, F., Bada, G., Cloetingh, S., 2006. Redistribution of recent collision push and ridge push in Central Europe: insights from FEM modelling. *Geophys. J. Int.* 167 (2), 860–880, <http://dx.doi.org/10.1111/j.1365-246X.2006.02979.x>.
- Jarosiński, M., 1998. Contemporary stress field distortion in the Polish part of the Western Outer Carpathians and their basement. *Tectonophysics* 297 (1–4), 91–119, [http://dx.doi.org/10.1016/s0040-1951\(98\)00165-6](http://dx.doi.org/10.1016/s0040-1951(98)00165-6).
- Köhler, A., Weidle, C., Maupin, V., 2011. Directionality analysis and Rayleigh wave tomography of ambient seismic noise in southern Norway. *Geophys. J. Int.* 184 (1), 287–300, <http://dx.doi.org/10.1111/j.1365-246X.2010.04830.x>.
- Kaiser, A., Reicherter, K., Hübscher, C., Gajewski, D., 2005. Variation of the present-day stress field within the North German Basin—insights from thin shell FE modeling based on residual GPS velocities. *Tectonophysics* 397 (1–2), 55–72, <http://dx.doi.org/10.1016/j.tecto.2004.10.009>.
- Kolstrup, M.L., Maupin, V., 2013. A proterozoic boundary in southern Norway revealed by joint-inversion of P-receiver functions and surface waves. *Precambrian Res.* 238, 186–198, <http://dx.doi.org/10.1016/j.precamres.2013.10.004>.
- Korenaga, J., 2004. Mantle mixing and continental breakup magmatism. *Earth Planet. Sci. Lett.* 218 (3–4), 463–473, [http://dx.doi.org/10.1016/s0012-821x\(03\)00674-5](http://dx.doi.org/10.1016/s0012-821x(03)00674-5).
- Korenaga, J., Kelemen, P.B., 2000. Major element heterogeneity in the mantle source of the North Atlantic igneous province. *Earth Planet. Sci. Lett.* 184 (1), 251–268, [http://dx.doi.org/10.1016/s0012-821x\(00\)00308-3](http://dx.doi.org/10.1016/s0012-821x(00)00308-3).
- Kumar, P., Kind, R., Hanka, W., Wylegalla, K., Reigber, C., Yuan, X., Woelbern, I., Schwintzer, P., Fleming, K., Dahl-Jensen, T., Larsen, T.B., Schweitzer, J., Priestley, K., Gudmundsson, O., et al., 2005. The lithosphere–asthenosphere boundary in the North-west Atlantic region. *Earth Planetary Sci. Lett.* 236 (1–2), 249–257, <http://dx.doi.org/10.1016/j.epsl.2005.05.029>.
- Kumar, P., Kind, R., Priestley, K., Dahl-Jensen, T., 2007. Crustal structure of Iceland and Greenland from receiver function studies. *J. Geophys. Res.: Solid Earth* 112 (B3), <http://dx.doi.org/10.1029/2005jb003991>.
- Lachenbruch, A.H., Morgan, P., 1990. Continental extension, magmatism and elevation; formal relations and rules of thumb. *United States Geol. Survey*, 39–62.
- Larsen, H.C., Saunders, A.D., 1998. Tectonism and volcanism at the Southeast Greenland Rifted Margin: a record of plume impact and later continental rapture. *Proceedings of the Ocean Drilling Program, Scientific Results*.
- Larsen, R.B., Tegner, C., 2006. Pressure conditions for the solidification of the Skæragaard intrusion: eruption of East Greenland flood basalts in less than 300,000 years. *Lithos* 92 (1–2), 181–197, <http://dx.doi.org/10.1016/j.lithos.2006.03.032>.
- Laske, G., Masters, G., Ma, Z., Pasquano, M., 2013. Update on CRUST1.0—a 1-degree Global Model of Earth's Crust. *Geophys. Res. Abstr.*
- Leslie, A.G., Smith, M., Scoper, N.J., 2008. Laurentian margin evolution and the Caledonian orogeny—a template for Scotland and East Greenland. In: *The Greenland Caledonides GSA Memoirs 202. The Geological Society of America*.
- Lidmar-Bergström, K., Näslund, J.O., 2002. Landforms and uplift in Scandinavia. *Geol. Soc. Lond. Special Publ.* 196 (1), 103–116, <http://dx.doi.org/10.1144/GSL.SP.2002.196.01.07>.
- Lithgow-Bertelloni, C., Guynn, J.H., 2004. Origin of the lithospheric stress field. *J. Geophys. Res.: Solid Earth* 109 (B1), B01408, <http://dx.doi.org/10.1029/2003jb002467>.

- Lund, J., 1989. A late Paleocene non-marine microflora from the interbasaltic coals of the Faeroe Islands, North Atlantic. *Bull. Geol. Soc. Denmark* 37, 181–203.
- Lundin, E.R., Doré, A.G., 2011. Hyperextension, serpentization, and weakening: a new paradigm for rifted margin compressional deformation. *Geology* 39 (4), 347–350, <http://dx.doi.org/10.1130/G31499.1>.
- Müller, B., Zoback, M.L., Fuchs, K., Mastin, L., Gregersen, S., Pavoni, N., Stephansson, O., Ljunggren, C., 1992. Regional patterns of tectonic stress in Europe. *J. Geophys. Res.: Solid Earth* 97 (B8), 11783–11803, <http://dx.doi.org/10.1029/91jb01096>.
- Müller, R.D., Sdrolias, M., Gaina, C., Roest, W.R., 2008. Age, spreading rates, and spreading asymmetry of the world's ocean crust. *Geochim. Geophys. Geosyst.* 9 (4), Q04006, <http://dx.doi.org/10.1029/2007gc001743>.
- MacLennan, J., Jones, S.M., 2006. Regional uplift, gas hydrate dissociation and the origins of the Paleocene-Eocene Thermal Maximum. *Earth Planet. Sci. Lett.* 245 (1–2), 65–80, <http://dx.doi.org/10.1016/j.epsl.2006.01.069>.
- Marotta, A.M., Bayer, U., Thybo, H., Scheck, M., 2002. Origin of the regional stress in the North German basin: results from numerical modelling. *Tectonophysics* 360 (1–4), 245–264, [http://dx.doi.org/10.1016/s0040-1951\(02\)00358-x](http://dx.doi.org/10.1016/s0040-1951(02)00358-x).
- Marquart, G., 1989. Isostatic topography and crustal depth corrections for the Fennoscandian geoid. *Tectonophysics* 169 (1–3), 67–77, [http://dx.doi.org/10.1016/0040-1951\(89\)90184-4](http://dx.doi.org/10.1016/0040-1951(89)90184-4).
- Maupin, V., Agostini, A., Artemieva, I., Balling, N., Beekman, F., Ebbing, J., England, R.W., Frassetto, A., Gradmann, S., Jacobsen, B.H., Köhler, A., Kvarven, T., Medhus, A.B., Mjelde, R., et al., 2013. The deep structure of the Scandes and its relation to tectonic history and present-day topography. *Tectonophysics* 602, 15–37, <http://dx.doi.org/10.1016/j.tecto.2013.03.010>.
- McKenzie, D., Bickle, M.J., 1988. The volume and composition of melt generated by extension of the lithosphere. *J. Petrol.* 29 (3), 625–679, <http://dx.doi.org/10.1093/petrology/29.3.625>.
- McKenzie, D., Jackson, J., Priestley, K., 2005. Thermal structure of oceanic and continental lithosphere. *Earth Planet. Sci. Lett.* 233 (3–4), 337–349, <http://dx.doi.org/10.1016/j.epsl.2005.02.005>.
- Medhus, A.B., Balling, N., Jacobsen, B.H., Weidle, C., England, R.W., Kind, R., Thybo, H., Voss, P., 2012. Upper-mantle structure beneath the Southern Scandes Mountains and the Northern Tornquist Zone revealed by P-wave traveltimes tomography. *Geophys. J. Int.* 189 (3), 1315–1334, <http://dx.doi.org/10.1111/j.1365-246x.2012.05449.x>.
- Medvedev, S., Hartz, E.H., 2015. Evolution of topography of post-Devonian Scandinavia: effects and rates of erosion. *Geomorphology* 231, 229–245, <http://dx.doi.org/10.1016/j.geomorph.2014.12.010>.
- Medvedev, S., Hartz, E.H., Podladchikov, Y.Y., 2008. Vertical motions of the fjord regions of central East Greenland: impact of glacial erosion, deposition, and isostasy. *Geology* 36 (7), 539–542, <http://dx.doi.org/10.1130/G24638A.1>.
- Medvedev, S., Souche, A., Hartz, E.H., 2013. Influence of ice sheet and glacial erosion on passive margins of Greenland. *Geomorphology* 193, 36–46, <http://dx.doi.org/10.1016/j.geomorph.2013.03.029>.
- Meyer, R., van Wijk, J., Gernigon, L., 2007. The North Atlantic Igneous Province: a review of models for its formation. *Geol. Soc. Am. Spec. Pap.* 430, 525–552, [http://dx.doi.org/10.1130/2007.2430\(26\)](http://dx.doi.org/10.1130/2007.2430(26)).
- Molnar, P., England, P.C., Jones, C.H., 2015. Mantle dynamics, isostasy, and the support of high terrain. *J. Geophys. Res.: Solid Earth*, <http://dx.doi.org/10.1002/2014jb011724> (2014JB011724).
- Morgan, W.J., 1971. Convection plumes in the lower mantle. *Nature* 230 (5288), 42–43, <http://dx.doi.org/10.1038/230042a0>.
- Moucha, R., Forte, A.M., 2011. Changes in African topography driven by mantle convection. *Nat. Geosci.* 4 (10), 707–712, <http://dx.doi.org/10.1038/ngeo1235>.
- Naliboff, J.B., Conrad, C.P., Lithgow-Bertelloni, C., 2009. Modification of the lithospheric stress field by lateral variations in plate-mantle coupling. *Geophys. Res. Lett.* 36 (22), <http://dx.doi.org/10.1029/2009gl040484>, p. L22307.
- Naliboff, J.b., Lithgow-Bertelloni, C., Ruff, L.j., de Koker, N., 2012. The effects of lithospheric thickness and density structure on Earth's stress field: geophysical Journal International. *Geophys. J. Int.* 188 (1), 1–17, <http://dx.doi.org/10.1111/j.1365-246X.2011.05248.x>.
- Neves, M.C., Fernandes, R.M., Adam, C., 2014. Refined models of gravitational potential energy compared with stress and strain rate patterns in Iberia. *J. Geodyn.* 81, 91–104, <http://dx.doi.org/10.1016/j.jog.2014.07.010>.
- Nielsen, S.B., Stephenson, R., Thomsen, E., 2007. Dynamics of Mid-Palaeocene North Atlantic rifting linked with European intra-plate deformations. *Nature* 450 (7172), 1071–1074, <http://dx.doi.org/10.1038/nature06379>.
- Nielsen, S.B., Gallagher, K., Leighton, C., Balling, N., Svenningsen, L., Jacobsen, B.H., Thomsen, E., Nielsen, O.B., Heilmann-Clausen, C., Egholm, D.L., Summerfield, M.A., Clausen, O.R., Piotrowski, J.A., Thorsen, M.R., et al., 2009. The evolution of western Scandinavian topography: a review of Neogene uplift versus the ICE (isostasy-climate-erosion) hypothesis. *J. Geodyn.* 47 (2–3), 72–95, <http://dx.doi.org/10.1016/j.jog.2008.09.001>.
- Nielsen, S.B., Stephenson, R., Schiffer, C., 2014. Deep controls on intraplate basin inversion. In: *Intraplate Earthquakes*. University Press, Cambridge.
- Nirnengarten, M., Gernigon, L., Manatschal, G., 2014. Lower crustal bodies in the More volcanic rifted margin: geophysical determination and geological implications. *Tectonophysics* 636, 143–157, <http://dx.doi.org/10.1016/j.tecto.2014.08.004>.
- Pascal, C., Cloetingh, S.A.P.L., 2009. Gravitational potential stresses and stress field of passive continental margins: insights from the south-Norway shelf. *Earth Planet. Sci. Lett.* 277 (3–4), 464–473, <http://dx.doi.org/10.1016/j.epsl.2008.11.014>.
- Pascal, C., Gabrielsen, R.H., 2001. Numerical modeling of Cenozoic stress patterns in the mid-Norwegian margin and the northern North Sea. *Tectonics* 20 (4), 585–599, <http://dx.doi.org/10.1029/2001TC900007>.
- Pascal, C., Olesen, O., 2009. Are the Norwegian mountains compensated by a mantle thermal anomaly at depth? *Tectonophysics* 475 (1), 160–168, <http://dx.doi.org/10.1016/j.tecto.2009.01.015>.
- Pedersen, V.K., Egholm, D.L., Nielsen, S.B., 2010. Alpine glacial topography and the rate of rock column uplift: a global perspective. *Geomorphology* 122 (1–2), 129–139, <http://dx.doi.org/10.1016/j.geomorph.2010.06.005>.
- Pedersen, V.K., Nielsen, S.B., Gallagher, K., 2012. The post-orogenic evolution of the Northeast Greenland Caledonides constrained from apatite fission track analysis and inverse geodynamic modelling. *Tectonophysics* 530–531, 318–330, <http://dx.doi.org/10.1016/j.tecto.2012.01.018>.
- Pedersen, V.K., Nielsen, S.B., Gallagher, K., 2013. Reply to: the mountains of North-East Greenland are not remnants of the Caledonian topography. A comment on Pedersen et al (2012). *Tectonophysics* 589, 239–244, <http://dx.doi.org/10.1016/j.tecto.2013.01.007>.
- Petrunin, G.I., Popov, V.G., 1995. Temperature dependence of lattice thermal conductivity of Earth's mineral substance. *Phys. Solid Earth* 30 (7/8), p. 617–623.
- Pollack, H.N., Chapman, D.S., 1977. On the regional variation of heat flow, geotherms, and lithospheric thickness. *Tectonophysics* 38 (3–4), 279–296, [http://dx.doi.org/10.1016/0040-1951\(77\)90215-3](http://dx.doi.org/10.1016/0040-1951(77)90215-3).
- Ranalli, G., 1995. *Rheology of the Earth*. Springer Science & Business Media.
- Rawlinson, N., Fichtner, A., Cambridge, M., Young, M.K., 2014. *Chapter one—seismic tomography and the assessment of uncertainty*. In: Dmowska, R. (Ed.), *Advances in Geophysics*. Elsevier, pp. 1–76.
- Ren, S., Faleide, J.I., Eldholm, O., Skogseid, J., Gladstein, F., 2003. Late Cretaceous-Paleocene tectonic development of the NW Vøring Basin. *Mar. Petrol. Geol.* 20 (2), 177–206, [http://dx.doi.org/10.1016/S0264-8172\(03\)00005-9](http://dx.doi.org/10.1016/S0264-8172(03)00005-9).
- Rickers, F., Fichtner, A., Trampert, J., 2013. The Iceland–Jan Mayen plume system and its impact on mantle dynamics in the North Atlantic region: evidence from full-waveform inversion. *Earth Planet. Sci. Lett.* 367, 39–51, <http://dx.doi.org/10.1016/j.epsl.2013.02.022>.
- Roberts, D.G., Bally, A.W. (Eds.), 2012. *Elsevier, Amsterdam, Boston*.
- Roberts, A.M., Lundin, E.R., Kusznir, N.J., 1997. Subsidence of the Vøring Basin and the influence of the Atlantic continental margin. *J. Geol. Soc.* 154 (3), 551–557, <http://dx.doi.org/10.1144/gsjgs.154.3.0551>.
- Roberts, D., 2003. The Scandinavian Caledonides: event chronology, palaeogeographic settings and likely modern analogues. *Tectonophysics* 365 (1–4), 283–299, [http://dx.doi.org/10.1016/s0040-1951\(03\)00026-x](http://dx.doi.org/10.1016/s0040-1951(03)00026-x).
- Rosenbaum, G., Lister, G.S., Duboz, C., 2002. Relative motions of Africa, Iberia and Europe during Alpine orogeny. *Tectonophysics* 359 (1–2), 117–129, [http://dx.doi.org/10.1016/s0040-1951\(02\)00442-0](http://dx.doi.org/10.1016/s0040-1951(02)00442-0).
- Saunders, A.D., Fitton, J.G., Kerr, A.C., Norry, M.J., Kent, R.W., 1997. *The North Atlantic Igneous Province*. In: honey, J.J., Coffin, M.F. (Eds.), *Large Igneous Provinces: Continental, Oceanic, and Planetary Flood Volcanism*. American Geophysical Union, 45–93.
- Schaeffer, A.J., Lebedev, S., 2013. Global shear speed structure of the upper mantle and transition zone. *Geophys. J. Int.* 194 (1), 417–449, <http://dx.doi.org/10.1093/gji/gjt095>.
- Schiffer, C., Balling, N., Jacobsen, B.H., Stephenson, R.A., Nielsen, S.B., 2014. Seismological evidence for a fossil subduction zone in the East Greenland Caledonides. *Geology* 42 (4), 311–314, <http://dx.doi.org/10.1130/G35244.1>.
- Schiffer, C., Jacobsen, B.H., Balling, N., Ebbing, J., Nielsen, S.B., 2015a. The East Greenland Caledonides—teleseismic signature, gravity and isostasy. *Geophys. J. Int.* 203 (2), 1400–1418, <http://dx.doi.org/10.1093/gji/gvz373>.
- Schiffer, C., Stephenson, R.A., Petersen, K.D., Nielsen, S.B., Jacobsen, B.H., Balling, N., Macdonald, D.I.M., 2015b. A sub-crustal piercing point for North Atlantic reconstructions and tectonic implications. *Geology* 43 (12), 1087–1090, <http://dx.doi.org/10.1130/G37245.1>.
- Skogseid, J., 1994. Dimensions of the Late Cretaceous-Paleocene Northeast Atlantic rift derived from Cenozoic subsidence. *Tectonophysics* 240 (1–4), 225–247, [http://dx.doi.org/10.1016/0040-1951\(94\)90274-7](http://dx.doi.org/10.1016/0040-1951(94)90274-7).
- Skogseid, J., Pedersen, T., Eldholm, O., Larsen, B.T., 1992. Tectonism and magmatism during NE Atlantic continental break-up: the Vøring Margin. *Geol. Soc. Lond. Special Publ.* 68 (1), 305–320, <http://dx.doi.org/10.1144/GSL.SP.1992.068.01.19>.
- Skogseid, J., Planke, S., Faleide, J.I., Pedersen, T., Eldholm, O., Neverdal, F., 2000. NE Atlantic continental rifting and volcanic margin formation. *Geol. Soc. Lond. Special Publ.* 167 (1), 295–326, <http://dx.doi.org/10.1144/GSL.SP.2000.167.01.12>.
- Stamfli, G.M., Kozur, H.W., 2006. Europe from the Variscan to the Alpine cycles. *Geol. Soc. Lond. Mem.* 32 (1), 57–82, <http://dx.doi.org/10.1144/GSL.MEM.2006.032.01.04>.
- Stein, C.A., Stein, S., 1992. A model for the global variation in oceanic depth and heat flow with lithospheric age. *Nature* 359 (6391), 123–129, <http://dx.doi.org/10.1038/359123a0>.
- Steinberger, B., Schmelting, H., Marquart, G., 2001. Large-scale lithospheric stress field and topography induced by global mantle circulation. *Earth Planet. Sci. Lett.* 186 (1), 75–91, [http://dx.doi.org/10.1016/S0012-821X\(01\)00229-1](http://dx.doi.org/10.1016/S0012-821X(01)00229-1).
- Steinberger, B., Spakman, W., Japsen, P., Torsvik, T.H., 2015. The key role of global solid-Earth processes in preconditioning Greenland's glaciation since the Pliocene. *Terra Nova* 27 (1), 1–8, <http://dx.doi.org/10.1111/ter.12133>.

- Stoker, M.S., Kimbell, G.S., McInroy, D.B., Morton, A.C., 2012. Eocene post-rift tectonostratigraphy of the Rockall Plateau Atlantic margin of NW Britain: linking early spreading tectonics and passive margin response. *Mar. Petrol. Geol.* 30 (1), 98–125, <http://dx.doi.org/10.1016/j.marpetgeo.2011.09.007>.
- Storey, M., Duncan, R.A., Tegner, C., 2007. Timing and duration of volcanism in the North Atlantic Igneous Province: implications for geodynamics and links to the Iceland hotspot. *Chem. Geol.* 241 (3–4), 264–281, <http://dx.doi.org/10.1016/j.chemgeo.2007.01.016>.
- Svennningsen, L., Balling, N., Jacobsen, B.H., Kind, R., Wylegalla, K., Schweitzer, J., 2007. Crustal root beneath the highlands of southern Norway resolved by teleseismic receiver functions. *Geophys. J. Int.* 170 (3), 1129–1138, <http://dx.doi.org/10.1111/j.1365-246X.2007.03402.x>.
- Tarantola, A., Valette, B., 1982. Generalized nonlinear inverse problems solved using the least squares criterion. *Rev. Geophys.* 20 (2), 219–232, <http://dx.doi.org/10.1029/RG020i002p00219>.
- Tassone, D.R., Holford, S.P., Stoker, M.S., Green, P., Johnson, H., Underhill, J.R., Hillis, R.R., 2014. Constraining Cenozoic exhumation in the Faroe-Shetland region using sonic transit time data. *Basin Res.* 26 (1), 38–72, <http://dx.doi.org/10.1111/bre.12052>.
- Tegner, C., Lesher, C.E., Larsen, L.M., Watt, W.S., 1998. Evidence from the rare-earth-element record of mantle melting for cooling of the Tertiary Iceland plume. *Nature* 395 (6702), 591–594, <http://dx.doi.org/10.1038/26956>.
- Torsvik, T.H., Carlos, D., Mosar, J., Cocks, L.R.M., Malme, T., 2002. Global reconstructions and North Atlantic palaeogeography 400Ma to recent. In: BATLAS—Mid Norway plate reconstructions atlas with global and Atlantic perspectives. Geological Survey of Norway, pp. 18–39.
- Turcotte, D.L., Schubert, G., 2002. *Geodynamics*. University Press, Cambridge.
- Weidle, C., Maupin, V., 2008. An upper-mantle S-wave velocity model for Northern Europe from Love and Rayleigh group velocities. *Geophys. J. Int.* 175 (3), 1154–1168, <http://dx.doi.org/10.1111/j.1365-246X.2008.03957.x>.
- Wu, P., Johnston, P., Lambeck, K., 1999. Postglacial rebound and fault instability in Fennoscandia. *Geophys. J. Int.* 139 (3), 657–670, <http://dx.doi.org/10.1046/j.1365-246X.1999.00963.x>.
- Xu, W., Lithgow-Bertelloni, C., Stixrude, L., Ritsema, J., 2008. The effect of bulk composition and temperature on mantle seismic structure. *Earth Planet. Sci. Lett.* 275 (1–2), 70–79, <http://dx.doi.org/10.1016/j.epsl.2008.08.012>.
- Zhu, H., Bozdağ, E., Peter, D., Tromp, J., 2012. Structure of the European upper mantle revealed by adjoint tomography. *Nat. Geosci.* 5 (7), 493–498, <http://dx.doi.org/10.1038/ngeo1501>.
- Ziegler, P.A., Dézes, P., 2006. Crustal evolution of Western and Central Europe. *Geol. Soc. Lond. Mem.* 32 (1), 43–56, <http://dx.doi.org/10.1144/GSL.MEM.2006.032.01.03>.
- Ziegler, P.A. (Ed.), 1990. *Geological Society of London, The Hague*.
- Zienkiewicz, 1977. *The Finite Element Method*. McGraw-Hill, Maidenhead, Berkshire, England.